

PREPARATION AND OPERATIONS OF THE MISSION PERFORMANCE
CENTRE (MPC) FOR THE COPERNICUS SENTINEL-3 MISSION

S3-A OLCI Cyclic Performance Report

Cycle No. 020

Start date: 11/07/2017

End date: 07/08/2017



*Mission
Performance
Centre*



Ref.: S3MPC.ACR.PR.01-020
Issue: 1.0
Date: 25/08/2017
Contract: 400011836/14/I-LG

Customer: ESA	Document Ref.: S3MPC.ACR.PR.01-020
Contract No.: 4000111836/14/I-LG	Date: 25/08/2017
	Issue: 1.0

Project:	PREPARATION AND OPERATIONS OF THE MISSION PERFORMANCE CENTRE (MPC) FOR THE COPERNICUS SENTINEL-3 MISSION		
Title:	S3-A OLCI Cyclic Performance Report		
Author(s):	OLCI ESLs		
Approved by:	L. Bourg, OLCI ESL Coordinator	Authorized by	Frédéric Rouffi, OPT Technical Performance Manager
Distribution:	ESA, EUMETSAT, S3MPC consortium		
Accepted by ESA	S. Dransfeld, MPC Deputy TO for OPT P. Féménias, MPC TO		
Filename	S3MPC.ACR.PR.01-020 - i1r0 - OLCI Cyclic Report 020.docx		

Disclaimer

The work performed in the frame of this contract is carried out with funding by the European Union. The views expressed herein can in no way be taken to reflect the official opinion of either the European Union or the European Space Agency.





Sentinel-3 MPC
S3-A OLCI Cyclic Performance Report
Cycle No. 020

Ref.: S3MPC.ACR.PR.01-020
 Issue: 1.0
 Date: 25/08/2017
 Page: iv

Table of content

TABLE OF CONTENT	IV
LIST OF FIGURES	V
1 INSTRUMENT MONITORING	1
1.1 CCD TEMPERATURES.....	1
1.2 RADIOMETRIC CALIBRATION	2
1.2.1 <i>Dark Offsets [OLCI-L1B-CV-230]</i>	4
1.2.2 <i>Instrument response and degradation modelling [OLCI-L1B-CV-250]</i>	7
1.2.3 <i>Ageing of nominal diffuser [OLCI-L1B-CV-240]</i>	14
1.2.4 <i>Updating of calibration ADF [OLCI-L1B-CV-260]</i>	17
1.2.5 <i>Radiometric Calibrations for sun azimuth angle dependency and Yaw Manoeuvres for Solar Diffuser on-orbit re-characterization [OLCI-L1B-CV-270 and OLCI-L1B-CV-280]</i>	18
1.3 SPECTRAL CALIBRATION [OLCI-L1B-CV-400].....	18
1.4 SIGNAL TO NOISE ASSESSMENT [OLCI-L1B-CV-620]	18
1.4.1 <i>SNR from Radiometric calibration data</i>	18
1.4.2 <i>SNR from EO data</i>	21
1.5 GEOMETRIC CALIBRATION/VALIDATION	21
2 OLCI LEVEL 1 PRODUCT VALIDATION	24
2.1 [OLCI-L1B-CV-300], [OLCI-L1B-CV-310] – RADIOMETRIC VALIDATION	24
2.1.1 <i>S3ETRAC Service</i>	24
2.1.2 <i>Radiometric validation with DIMITRI</i>	25
2.1.3 <i>Radiometric validation with OSCAR</i>	31
2.2 [OLCI-L1B-CV-320] – RADIOMETRIC VALIDATION WITH LEVEL 3 PRODUCTS.....	32
3 LEVEL 2 LAND PRODUCTS VALIDATION	36
3.1 [OLCI-L2LRF-CV-300].....	36
3.2 [OLCI-L2LRF-CV-410 & OLCI-L2LRF-CV-420] – CLOUD MASKING & SURFACE CLASSIFICATION FOR LAND PRODUCTS	36
3.3 VALIDATION OF INTEGRATED WATER VAPOUR OVER LAND	39
4 LEVEL 2 WATER PRODUCTS VALIDATION	40
4.1 [OLCI-L2-CV-210, OLCI-L2-CV-220] – VICARIOUS CALIBRATION OF THE NIR AND VIS BANDS.....	40
4.2 [OLCI-L2WLR-CV-300, OLCI-L2WLR-CV-310, OLCI-L2WLR-CV-32, OLCI-L2WLR-CV-330, OLCI-L2WLR-CV-340, OLCI-L2WLR-CV-350, OLCI-L2WLR-CV-360 AND OLCI-L2WLR-CV-370] – LEVEL 2 WATER-LEAVING REFLECTANCE PRODUCT VALIDATION.....	40
4.3 [OLCI-L2WLR-CV530] VALIDATION OF AEROSOL PRODUCT.....	40
5 LEVEL 2 SYN PRODUCTS VALIDATION	41
5.1 [SYN-L2-CV-100]	41
6 EVENTS	42
7 APPENDIX A	43

	<p>Sentinel-3 MPC</p> <p>S3-A OLCI Cyclic Performance Report</p> <p>Cycle No. 020</p>	<p>Ref.: S3MPC.ACR.PR.01-020</p> <p>Issue: 1.0</p> <p>Date: 25/08/2017</p> <p>Page: v</p>
--	--	---

List of Figures

Figure 1: long term monitoring of CCD temperatures using minimum value (top), time averaged values (middle), and maximum value (bottom) provided in the annotations of the Radiometric Calibration Level 1 products, for the Shutter frames, all radiometric calibrations so far. ----- 1

Figure 2: Same as Figure 1 for diffuser frames. ----- 2

Figure 3: Sun azimuth angles during acquired Radiometric Calibrations (diffuser frame) on top of nominal yearly cycle (black curve). Diffuser 1 with diamonds, diffuser 2 with crosses, 2016 acquisitions in blue, 2017 in red. ----- 3

Figure 4: Sun geometry during radiometric Calibrations on top of characterization ones (diffuser frame) 3

Figure 5: Dark Offset for band Oa1 (top) and Oa21 (bottom), all radiometric calibrations so far except the first one (orbit 183) for which the instrument was not thermally stable yet. ----- 4

Figure 6: map of periodic noise for the 5 cameras, for band Oa21. X-axis is detector number (East part, from 540 to 740, where the periodic noise occurs), Y-axis is the orbit number. The counts have been corrected from the west detectors mean value (not affected by periodic noise). Periodic noise amplitude is high in camera 2, 3 and 4. It is lower in camera 4 and small in camera 1. ----- 5

Figure 7: Dark Current for band Oa1 (top) and Oa21 (bottom), all radiometric calibrations so far except the first one (orbit 183) for which the instrument was not thermally stable yet. ----- 6

Figure 8: left column: ACT mean on 400 first detectors of Dark Current coefficients for spectral band Oa01 (top) and Oa21 (bottom). Right column: same as left column but for Standard deviation instead of mean. We see an increase of the DC level as a function of time especially for band Oa21. A possible explanation could be the increase of the number of hot pixels which is more important in Oa21 because this band is made of more CCD lines than band Oa01 and thus receives more cosmic rays impacts. It is known that cosmic rays degrade the structure of the CCD, generating more and more hot pixels at long term scales. ----- 6

Figure 9: Gain Coefficients for band Oa1 (top) and Oa21 (bottom), all diffuser 1 radiometric calibrations so far except the first one (orbit 183) for which the instrument was not thermally stable yet. ----- 7

Figure 10: camera averaged gain relative evolution with respect to “best geometry” calibration (22/11), as a function of elapsed time since launch; one curve for each band (see colour code on plots), one plot for each module. The star tracker anomaly fix (6/04/16) is represented by a vertical red dashed line. ---- 8

Figure 11: Camera-averaged instrument evolution since channel programming change (25/04/2016) and up to most recent calibration (22/07/2017) versus wavelength.----- 9

Figure 12: For the 5 cameras: Evolution model performance, as camera-average and standard deviation of ratio of Model over Data vs. wavelength, for each orbit of the test dataset, including 8 calibration in extrapolation, with a colour code for each calibration from blue (oldest) to red (most recent).-----10

Figure 13: model performance: ratio of model over data for all pixels (x axis) of all orbits (y axis), for channel Oa4. The outlying orbit #40 is that of 31/03/2017. -----11

	<p>Sentinel-3 MPC</p> <p>S3-A OLCI Cyclic Performance Report</p> <p>Cycle No. 020</p>	<p>Ref.: S3MPC.ACR.PR.01-020</p> <p>Issue: 1.0</p> <p>Date: 25/08/2017</p> <p>Page: vi</p>
--	--	--

Figure 14: Evolution model performance, as ratio of Model over Data vs. pixels, all cameras side by side, over the whole current calibration dataset (since instrument programming update), including 8 calibration in extrapolation, channels Oa1 to Oa6. -----12

Figure 15: same as Figure 14 for channels Oa7 to Oa14. -----13

Figure 16: same as Figure 14 for channels Oa15 to Oa21.-----14

Figure 17: diffuser 1 ageing for spectral band Oa01. We see strong ACT low frequency structures that are due to residual of BRDF modelling. -----15

Figure 18: same as Figure 17 for spectral band Oa16. We use this band in order to normalize other bands and remove the ACT structures due to residual of BRDF modelling. Normalized curve for spectral band Oa01 is presented in Figure 19. -----16

Figure 19: same as Figure 17 after normalization by band Oa16. Ageing of the diffuser 1 is now visible in the 5 cameras.-----16

Figure 20: Diffuser 1 ageing as a function of wavelength (or spectral band). Ageing is visible in spectral band #1 to #5. -----17

Figure 21: Camera averaged ageing (normalized by band Oa16) as a function of time. Linear fit for each camera is plotted. The slope (% loss per year) and the correlation coefficient -----17

Figure 22: Signal to Noise ratio as a function of the spectral band for the 5 cameras. These results have been computed from radiometric calibration data. All calibrations except first one (orbit 183) are presents with the colours corresponding to the orbit number (see legend). The SNR is very stable with time: the curves for all orbits are almost superimposed. The dashed curve is the ESA requirement. -----19

Figure 23: long-term stability of the SNR estimates from Calibration data, example of channel Oa1. -----20

Figure 24: histograms of geolocation errors for the along-track (left) and across-track (right) directions, example of 25/07/2017. -----22

Figure 25: georeferencing error in along-track (left) and across-track (right) directions for all the GCPs. 22

Figure 26: average and dispersion time series of the geolocation errors in along-track (blue) and across-track (red) directions over 15 months. -----23

Figure 27: summary of S3ETRAC products generation for OLCI (number of OLCI L1 products Ingested, yellow – number of S3ETRAC extracted products generated, blue – number of S3ETRAC runs without generation of output product (data not meeting selection requirements), green – number of runs ending in error, red, one plot per site type). -----25

Figure 28: Time-series of the elementary ratios (observed/simulated) signal from S3A/OLCI for (top to bottom) bands Oa03, Oa8 and Oa17 respectively over Six PICS Cal/Val sites. Dashed-green and orange lines indicate the 2% and 5% respectively. Error bars indicate the desert methodology uncertainty. -----27

Figure 29: The estimated gain values for S3A/OLCI over the 6 PICS sites identified by CEOS over the period April 2016 – July 2017 as a function of wavelength. Dashed-green and orange lines indicate the 2% and 5% respectively. Error bars indicate the desert methodology uncertainty. -----28

	<p>Sentinel-3 MPC</p> <p>S3-A OLCI Cyclic Performance Report</p> <p>Cycle No. 020</p>	<p>Ref.: S3MPC.ACR.PR.01-020</p> <p>Issue: 1.0</p> <p>Date: 25/08/2017</p> <p>Page: vii</p>
--	--	---

Figure 30: Time-series of the elementary ratios (observed/simulated) signal from (black) S2A/MSI, (blue) S3A/OLCI and (Cyan) Aqua/MODIS for (band Oa17: 865nm and Oa08: 665 nm over ALGERIA5 and LIBYA1 sites. Dashed-green and orange lines indicate the 2% and 5% respectively. Error bars indicate the desert methodology uncertainty.-----29

Figure 31: The estimated gain values (observed-signal /simulated-signal) averaged over the period April-August 2017 from (black)S2A/MSI, (blue) S3A/OLCI and (Cyan) Aqua/MODIS over ALGERIA5 and LIBYA1 sites as function of wavelength. Dashed-green and orange lines indicate the 2% and 5% respectively. Error bars indicate the desert methodology uncertainty.-----30

Figure 32: The estimated gain values for S3A/OLCI over the 6 Ocean CalVal sites (Atl-NW_Optimum, Atl-SW_Optimum, Pac-NE_Optimum, Pac-NW_Optimum, SPG_Optimum and SIO_Optimum) over the period December 2016 – August 2017 as a function of wavelength. Dashed-green, and orange lines indicate the 2%, 5% respectively. Error bars indicate the methodology uncertainty.-----31

Figure 33: Illustration of the comparison of the water reflectances retrieved under various geometry conditions (air mass) in the same day, in the Arctic region. -----33

Figure 34: self-consistency results of OLCI and MERIS Rw412 products. Each plot shows the variation of the water reflectance with the reference observation (the observation at minimal air mass) from the same day. The slope of the fit gives the dependency of Rw412 on the air mass. -----34

Figure 35: Summary of the self-consistency slopes (see previous figure) for each band, and for each product. -----35

Figure 36: Level 1 FR product-----37

Figure 37: Level 1 FR product with corresponding Level 2 flags for cloud, cloud ambiguous, cloud margin & snow -----38

Figure 38: Level 2 flag legend-----38



1 Instrument monitoring

1.1 CCD temperatures

The monitoring of the CCD temperatures is based on MPMF data extractions not yet operational. In the meantime, we monitor the CCD temperatures on the long-term using Radiometric Calibration Annotations (see Figure 1). Variations are very small (0.09 C peak-to-peak) and no trend can be identified. Data from current cycle (rightmost data points) do not show any specificity.

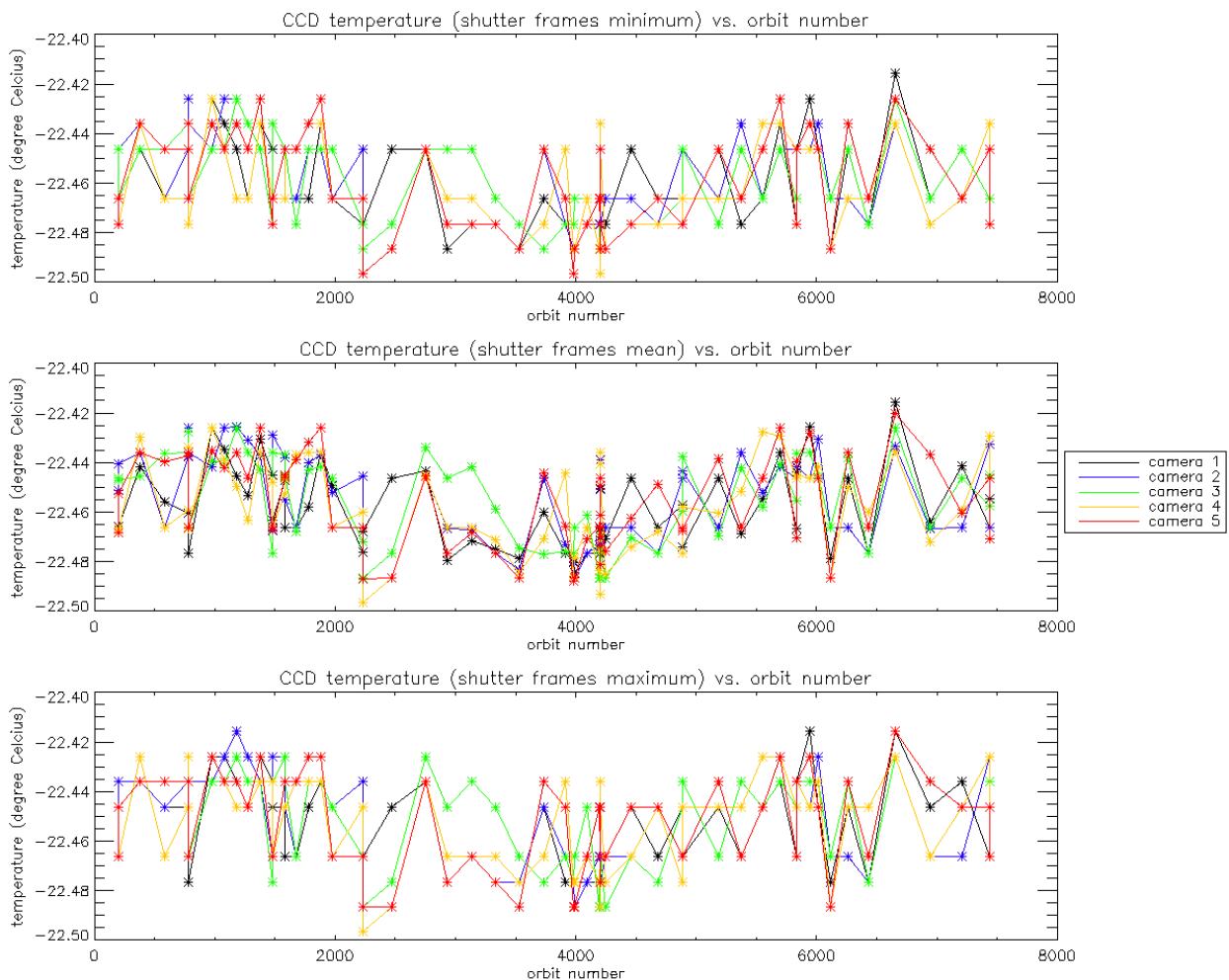


Figure 1: long term monitoring of CCD temperatures using minimum value (top), time averaged values (middle), and maximum value (bottom) provided in the annotations of the Radiometric Calibration Level 1 products, for the Shutter frames, all radiometric calibrations so far.

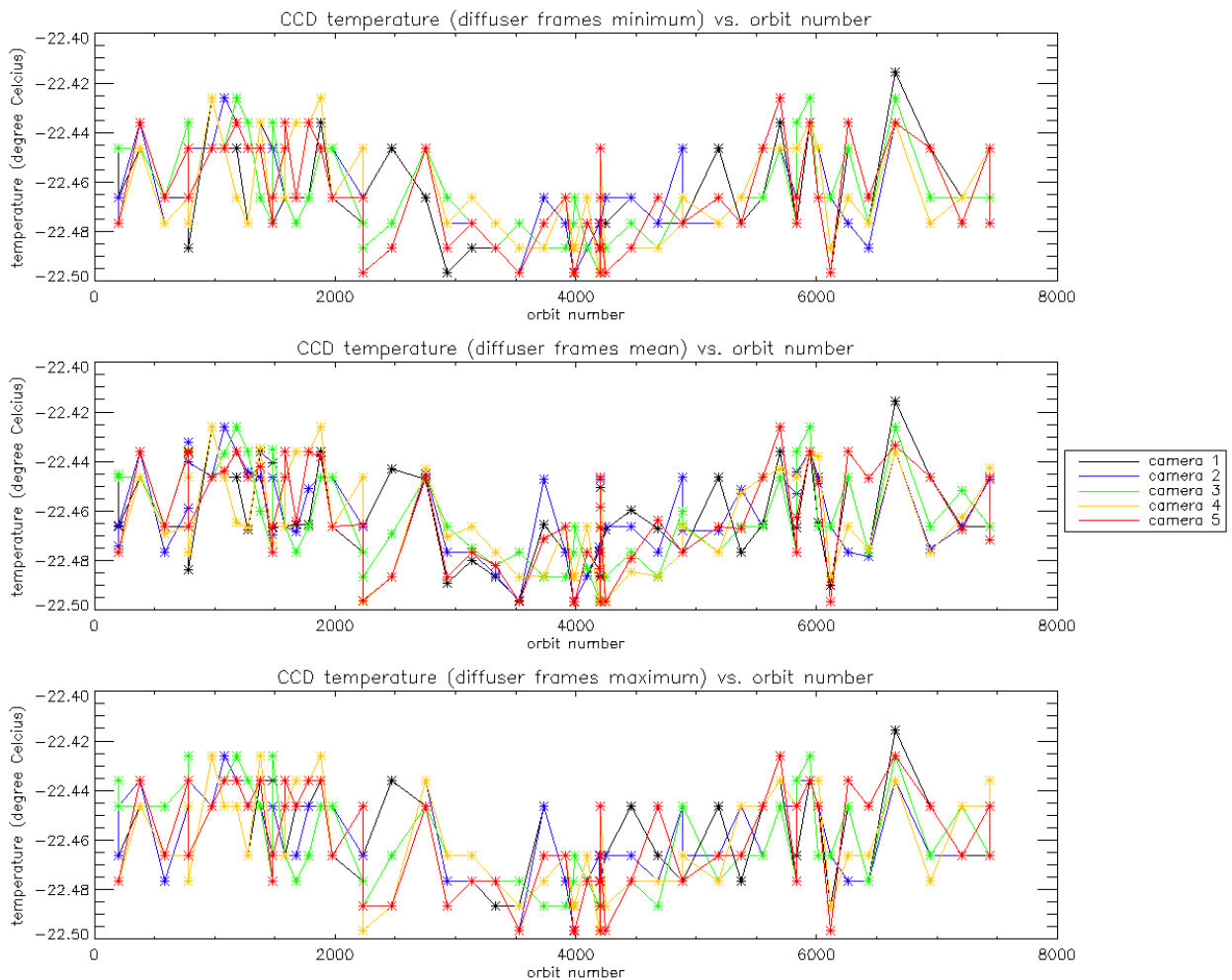


Figure 2: Same as Figure 1 for diffuser frames.

1.2 Radiometric Calibration

Two OLCI Radiometric Calibration Sequences have been acquired during Cycle 020:

- ❖ S04 sequence (diffuser 1) on 22/07/2017 08:09 to 08:11 (absolute orbit 7437)
- ❖ S05 sequence (diffuser 2) on 22/07/2017 09:50 to 09:52 (absolute orbit 7438)

The acquired Sun azimuth angles are presented on below, on top of the nominal values without Yaw Manoeuvre (i.e. with nominal Yaw Steering control of the satellite).

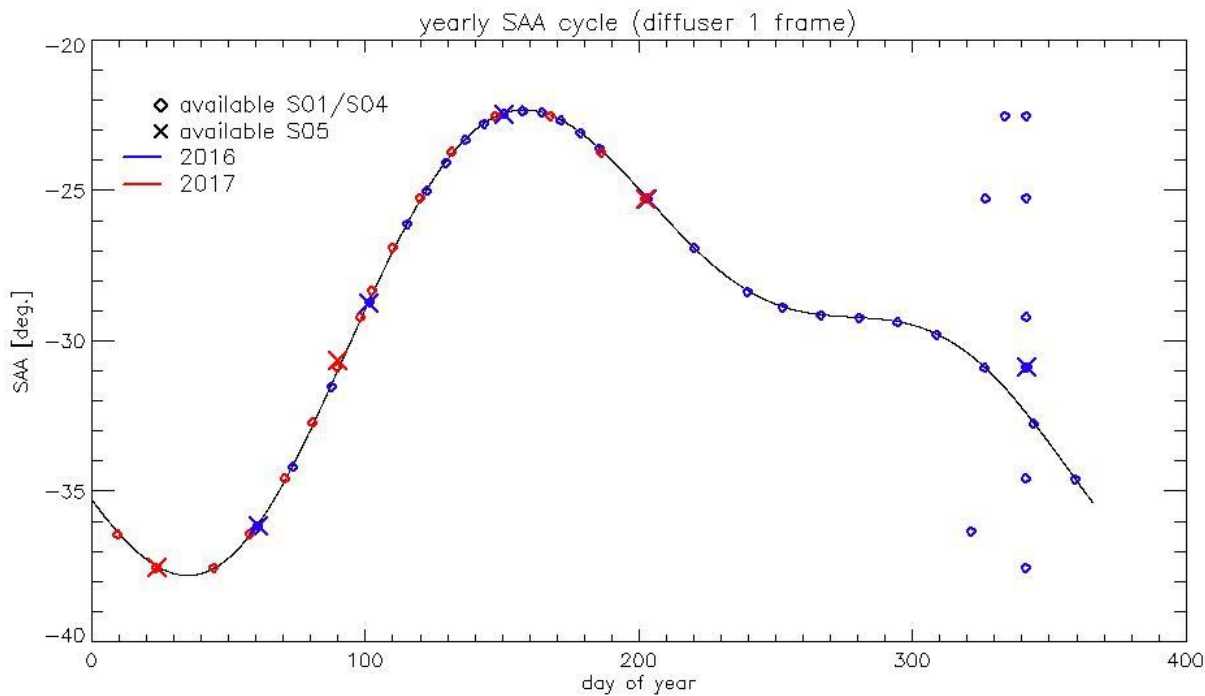


Figure 3: Sun azimuth angles during acquired Radiometric Calibrations (diffuser frame) on top of nominal yearly cycle (black curve). Diffuser 1 with diamonds, diffuser 2 with crosses, 2016 acquisitions in blue, 2017 in red.

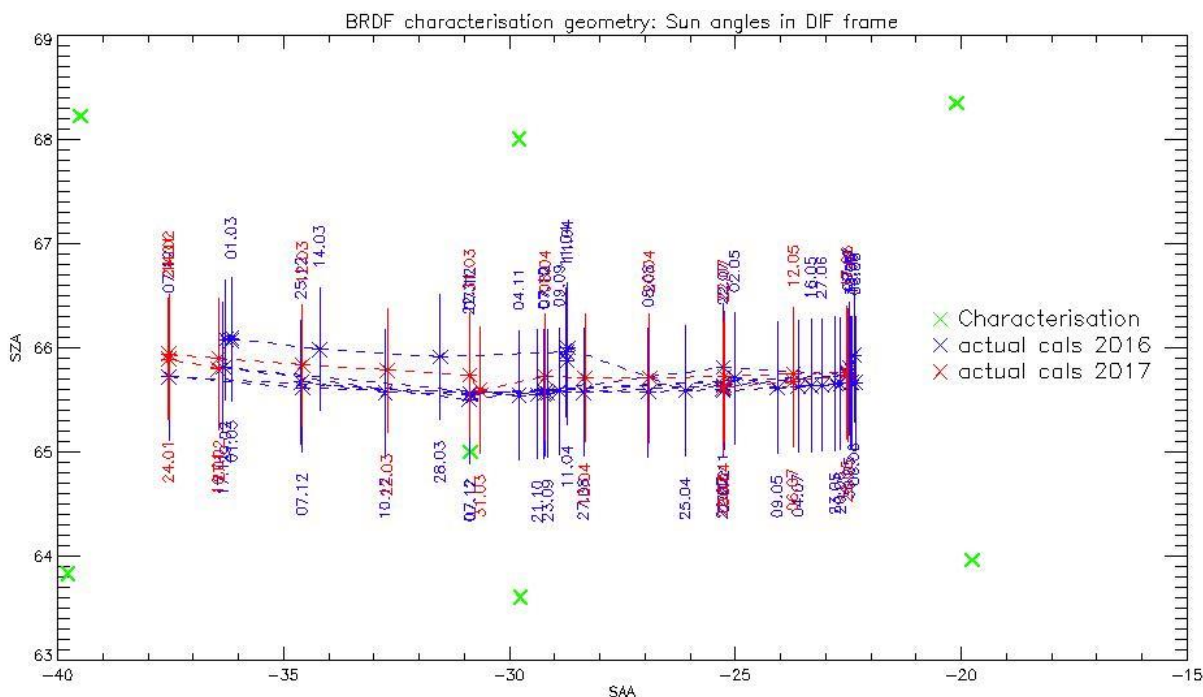


Figure 4: Sun geometry during radiometric Calibrations on top of characterization ones (diffuser frame)

This section presents the overall monitoring of the parameters derived from radiometric calibration data and highlights, if present, specificity of current cycle data.



1.2.1 Dark Offsets [OLCI-L1B-CV-230]

Dark offsets

Dark offsets are continuously affected by the global offset induced by the Periodic Noise on the OLCI convergence. Current Cycle calibrations are affected the same way as others. The amplitude of the shift varies with band and camera from virtually nothing (e.g. camera 2, band Oa1) to up to 5 counts (Oa21, camera 3). The Periodic Noise itself comes on top of the global shift with its known signature: high frequency oscillations with a rapid damp. This effect remains more or less stable with time in terms of amplitude, frequency and decay length, but its phase varies with time, introducing the global offset mentioned above.

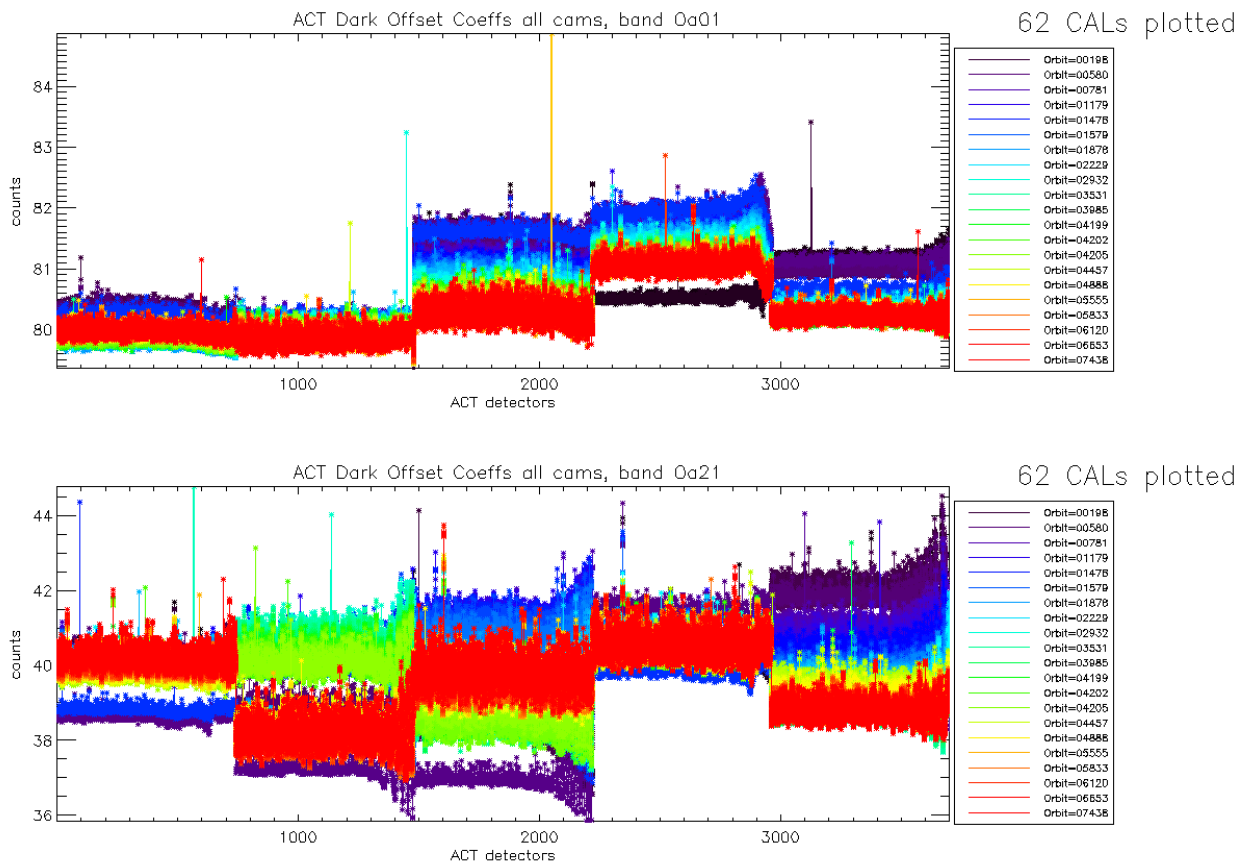


Figure 5: Dark Offset for band Oa1 (top) and Oa21 (bottom), all radiometric calibrations so far except the first one (orbit 183) for which the instrument was not thermally stable yet.

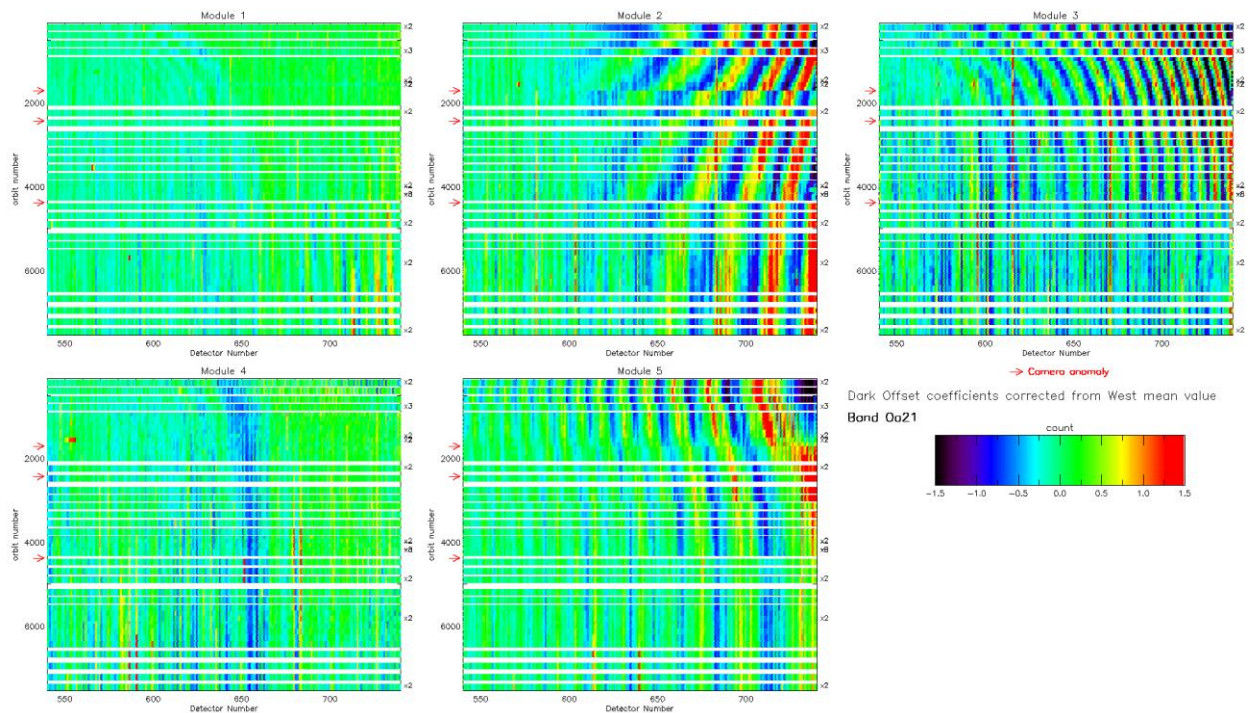


Figure 6: map of periodic noise for the 5 cameras, for band Oa21. X-axis is detector number (East part, from 540 to 740, where the periodic noise occurs), Y-axis is the orbit number. The counts have been corrected from the west detectors mean value (not affected by periodic noise). Periodic noise amplitude is high in camera 2, 3 and 4. It is lower in camera 4 and small in camera 1.

Looking at Figure 5 shows no significant evolution of this parameter during the current cycle. Figure 6 shows that since the last sudden PN change (phase and amplitude) caused by the camera-2 anomaly at orbit 4364 (18 December 2016), PN is nearly stabilized again. (See in particular cameras 2, 3 & 5).

Dark Currents

Dark Currents are not affected by the global offset of the Dark Offsets, thanks to the clamping to the average blind pixels value. However, the oscillations of Periodic Noise remain visible. There is no significant evolution of this parameter during the current cycle.

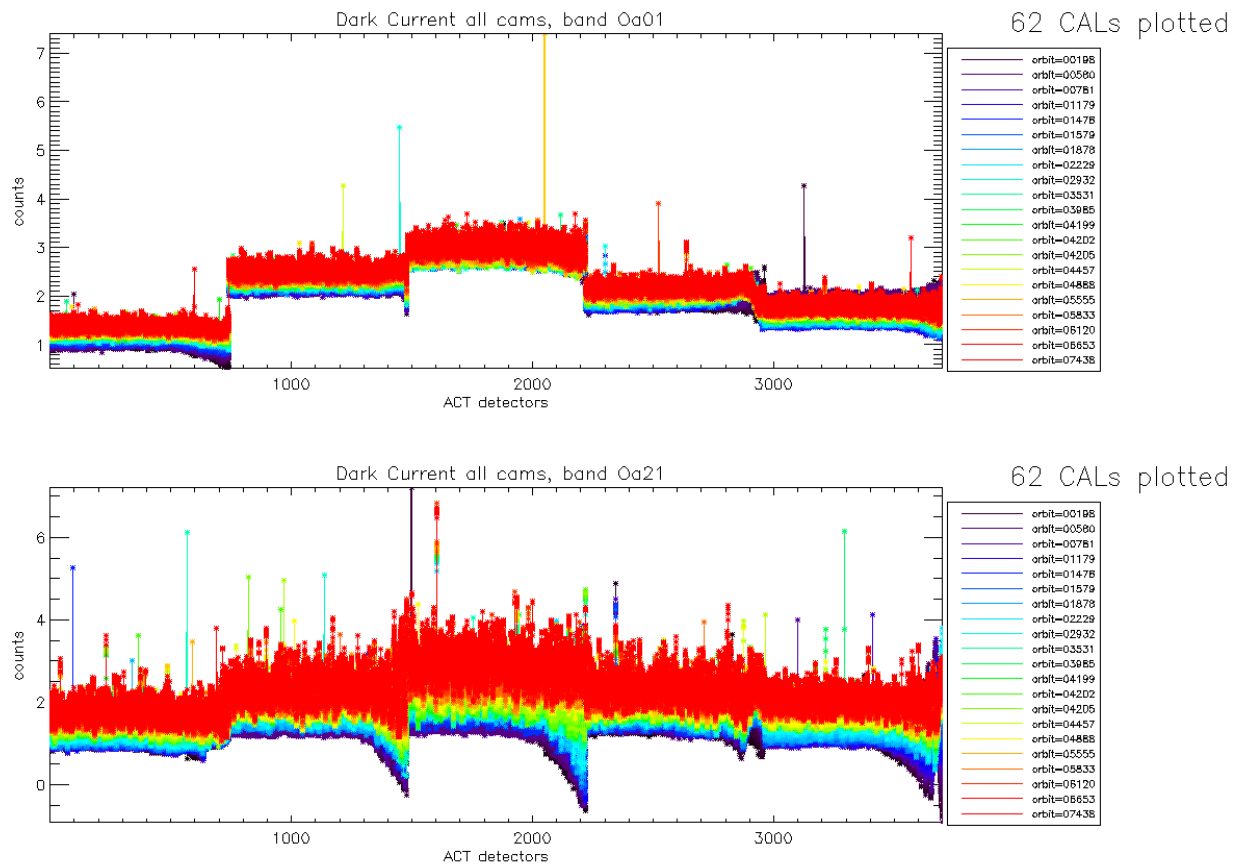


Figure 7: Dark Current for band Oa1 (top) and Oa21 (bottom), all radiometric calibrations so far except the first one (orbit 183) for which the instrument was not thermally stable yet.

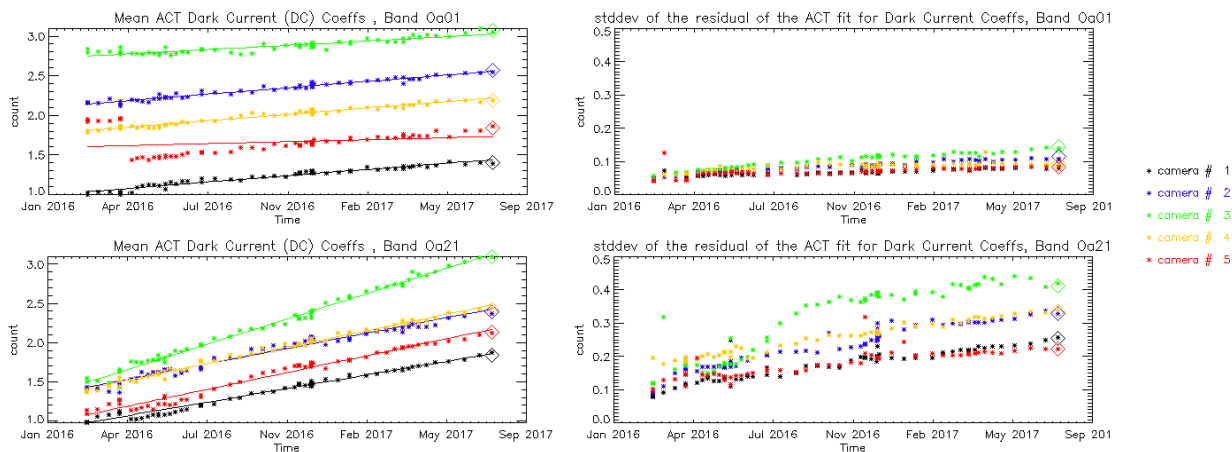


Figure 8: left column: ACT mean on 400 first detectors of Dark Current coefficients for spectral band Oa01 (top) and Oa21 (bottom). Right column: same as left column but for Standard deviation instead of mean. We see an increase of the DC level as a function of time especially for band Oa21. A possible explanation could be the increase of the number of hot pixels which is more important in Oa21 because this band is made of more CCD lines than band Oa01 and thus receives more cosmic rays impacts. It is known that cosmic rays degrade the structure of the CCD, generating more and more hot pixels at long term scales.

1.2.2 Instrument response and degradation modelling [OLCI-L1B-CV-250]

1.2.2.1 Instrument response monitoring

Figure 9 below shows the gain coefficients of every pixel for two OLCI channels, Oa1 (400 nm) and Oa21 (1020 nm), highlighting the significant evolution of the instrument response since early mission.

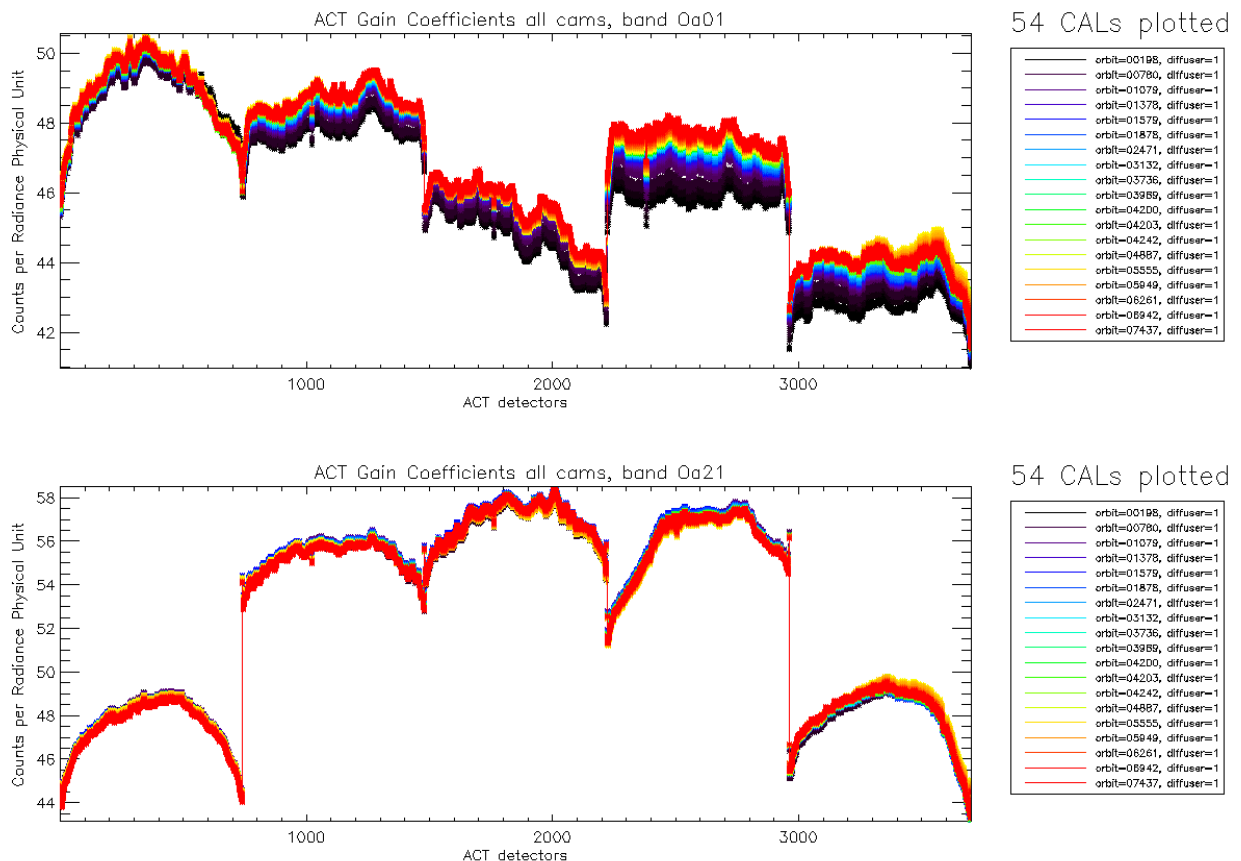


Figure 9: Gain Coefficients for band Oa1 (top) and Oa21 (bottom), all diffuser 1 radiometric calibrations so far except the first one (orbit 183) for which the instrument was not thermally stable yet.

The gains plotted in Figure 9, however are derived using the ground BRDF model – as the only one available in the operational processing software so far – which is known to suffer from illumination geometry dependent residual errors (see previous Cyclic Reports for more details). Consequently they are post-processed to replace the ground BRDF model by the in-flight version, based on Yaw Manoeuvres data, prior to determine the radiometric evolution.

Figure 10 displays a summary of the time evolution derived from post-processed gains: the cross-track average of the BRDF corrected gains is plotted as a function of time, for each module, relative to a given reference calibration (the 12/12/2016). It shows that, if a significant evolution occurred during the early mission, the trends tend to stabilize, with the exception of band 1 of camera 4.

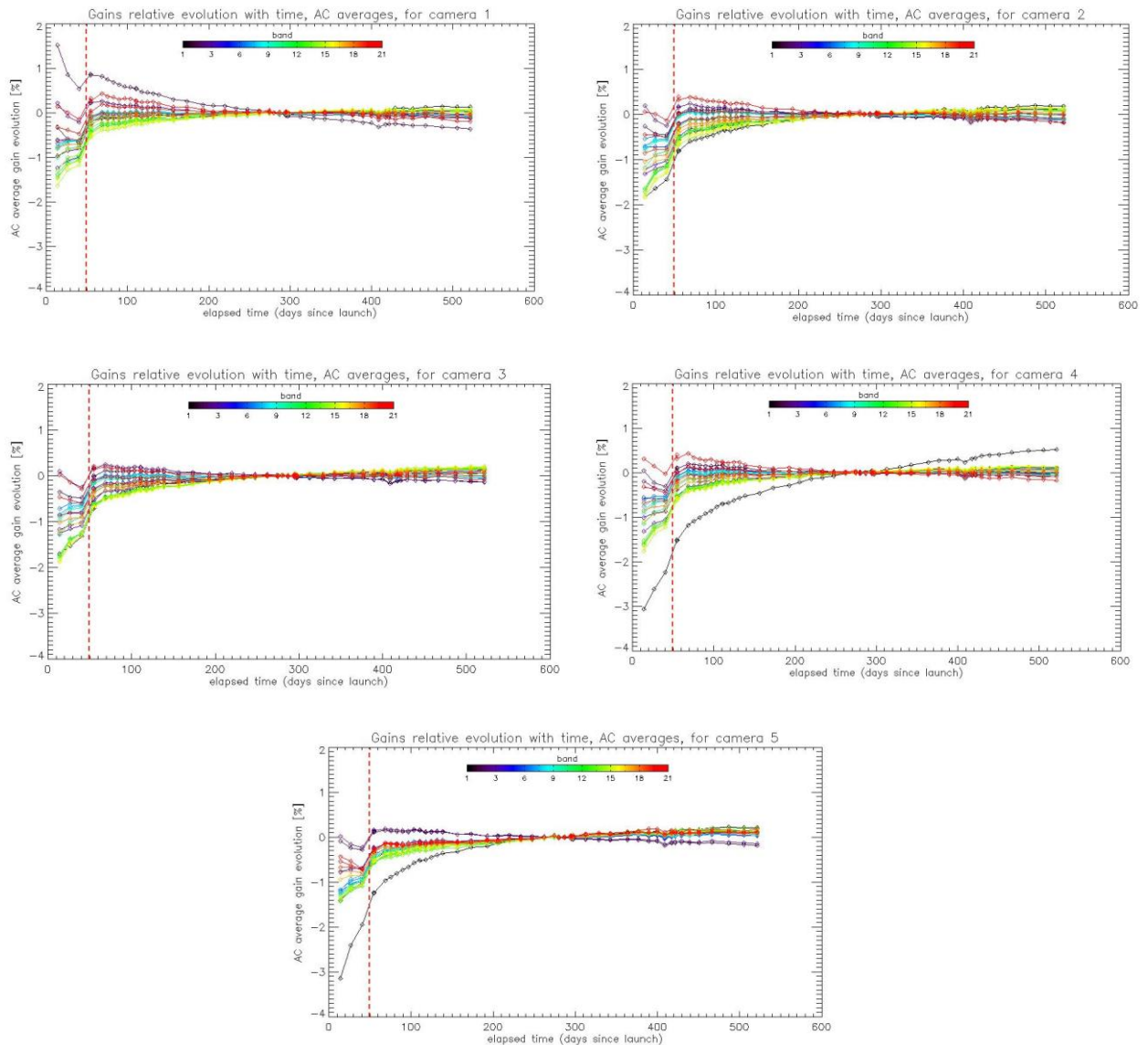


Figure 10: camera averaged gain relative evolution with respect to “best geometry” calibration (22/11), as a function of elapsed time since launch; one curve for each band (see colour code on plots), one plot for each module. The star tracker anomaly fix (6/04/16) is represented by a vertical red dashed line.

The behaviour over the first two months of mission, really different and highlighted by Figure 10, is explained by the Star Tracker software anomaly during which the attitude information provided by the platform was corrupted, preventing to compute a correct illumination geometry, with a significant impact on the gain computation.

1.2.2.2 Instrument evolution modelling

Thanks to the work done on the Yaw Manoeuvres Calibration acquisitions (see section 1.2.5) an upgraded diffuser BRDF model has been derived, allowing to get rid of the operational model dependency with Sun azimuth discussed above. This in turn allowed building a global gain database

corrected for BRDF error residuals. This database was used as the basis for the derivation of a long-term radiometric drift model.

This required a number of adaptations of the dedicated software for several reasons:

- 1) The upgraded BRDF model is not implemented in the Calibration processing software (IPF OL1-RC), thus the derived gains have to be corrected for BRDF in a post-processing step, on the (justified) assumption that the BRDF changes have a second order impact on the stray-light computation.
- 2) The observed instrument evolution does not follow the expected behaviour: a slow and smooth instrument sensitivity decrease, but on the contrary can show increase as well (see Figure 11))
- 3) The time period is not long enough to correctly model the evolution for cameras/channels for which it is very small: in this case the signal to noise ratio (e. g. due to diffuser speckle) is not high enough and the fit parameters that provide the best match are not physical. As a consequence, it may happen that, despite the model matches very well to the data, its use in extrapolation generates huge drifts that are very unlikely to occur. A post-processing is thus necessary to identify and update those cases.

The model has been derived from the dataset ranging from 26/04/2016 to 12/03/2017, so that the validation dataset now includes 8 calibrations over 2.5 months for performance estimation, including the calibrations acquired during current cycle.

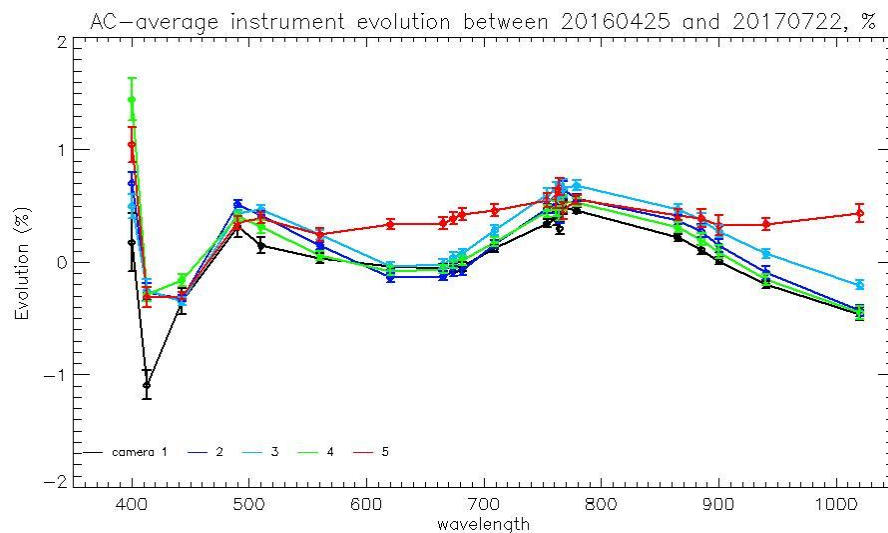


Figure 11: Camera-averaged instrument evolution since channel programming change (25/04/2016) and up to most recent calibration (22/07/2017) versus wavelength.

Once these steps are completed, the model performance over the complete dataset (including 8 calibrations in extrapolation over up to 2.5 months) is better than 0.2% except at very specific cases: few isolated pixels in about half of the bands, and two specific features in camera 5 for channels Oa8 and Oa21 that cannot be fitted with a bounded exponential model. The overall performance at each orbit is



shown on Figure 12 as the average and standard deviation of the model over data ratio as a function of wavelength, for each orbit in order to highlight a possible extrapolation issue. If the figure shows an outlying orbit, it must be stressed that it is NOT the most recent, excluding a systematic drift in extrapolation, as proved by Figure 13.

Finally, Figure 14 to Figure 16 show the detail of the model performance, with across-track plots of the model over data ratios at each orbit, one plot for each channel.

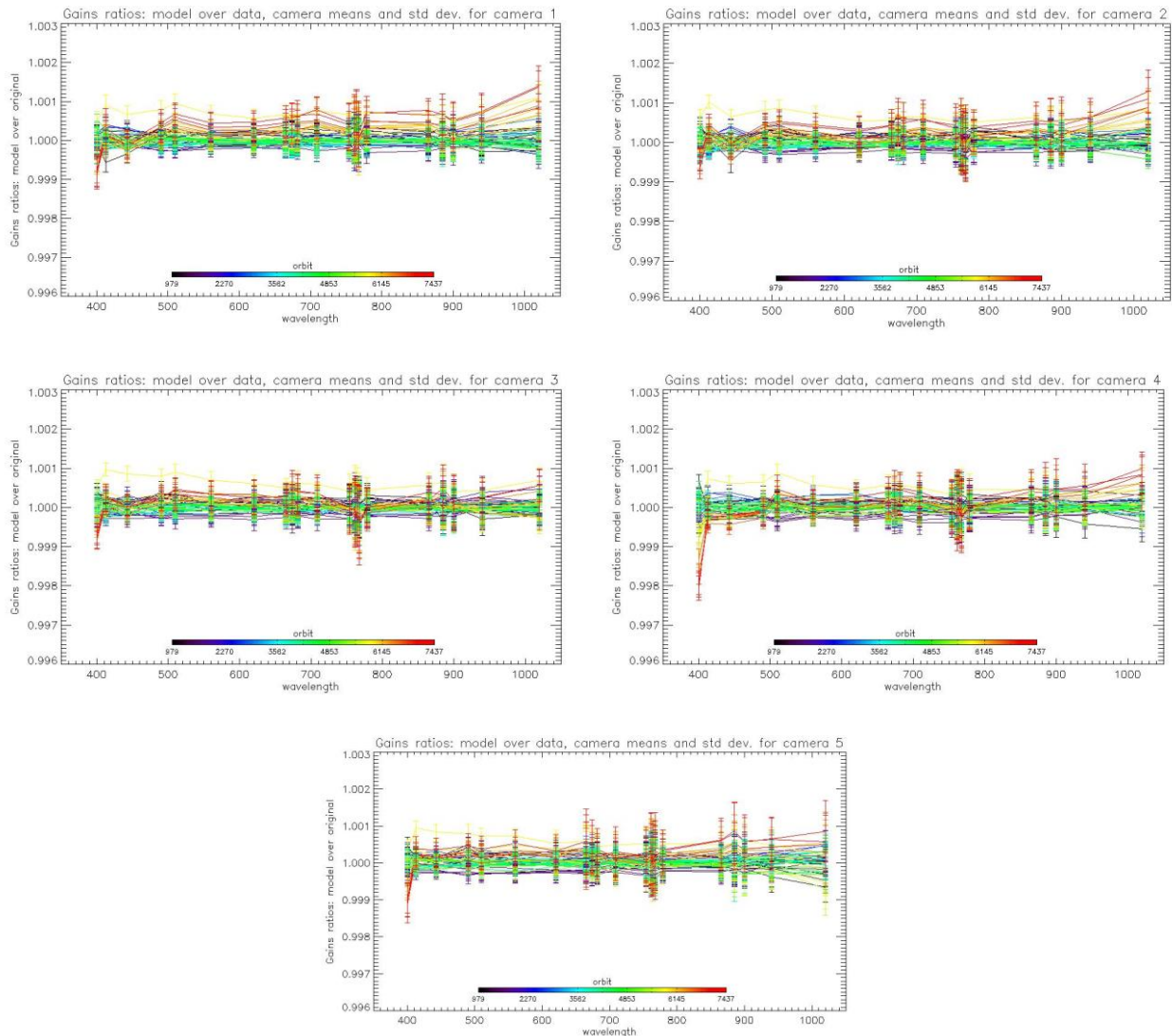


Figure 12: For the 5 cameras: Evolution model performance, as camera-average and standard deviation of ratio of Model over Data vs. wavelength, for each orbit of the test dataset, including 8 calibration in extrapolation, with a colour code for each calibration from blue (oldest) to red (most recent).



Sentinel-3 MPC
S3-A OLCI Cyclic Performance Report
Cycle No. 020

Ref.: S3MPC.ACR.PR.01-020
Issue: 1.0
Date: 25/08/2017
Page: 11

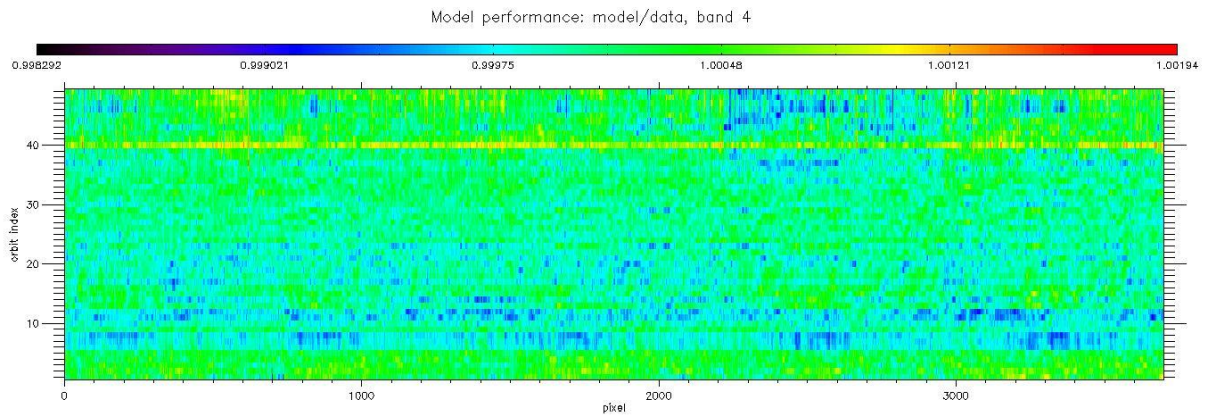


Figure 13: model performance: ratio of model over data for all pixels (x axis) of all orbits (y axis), for channel Oa4. The outlying orbit #40 is that of 31/03/2017.

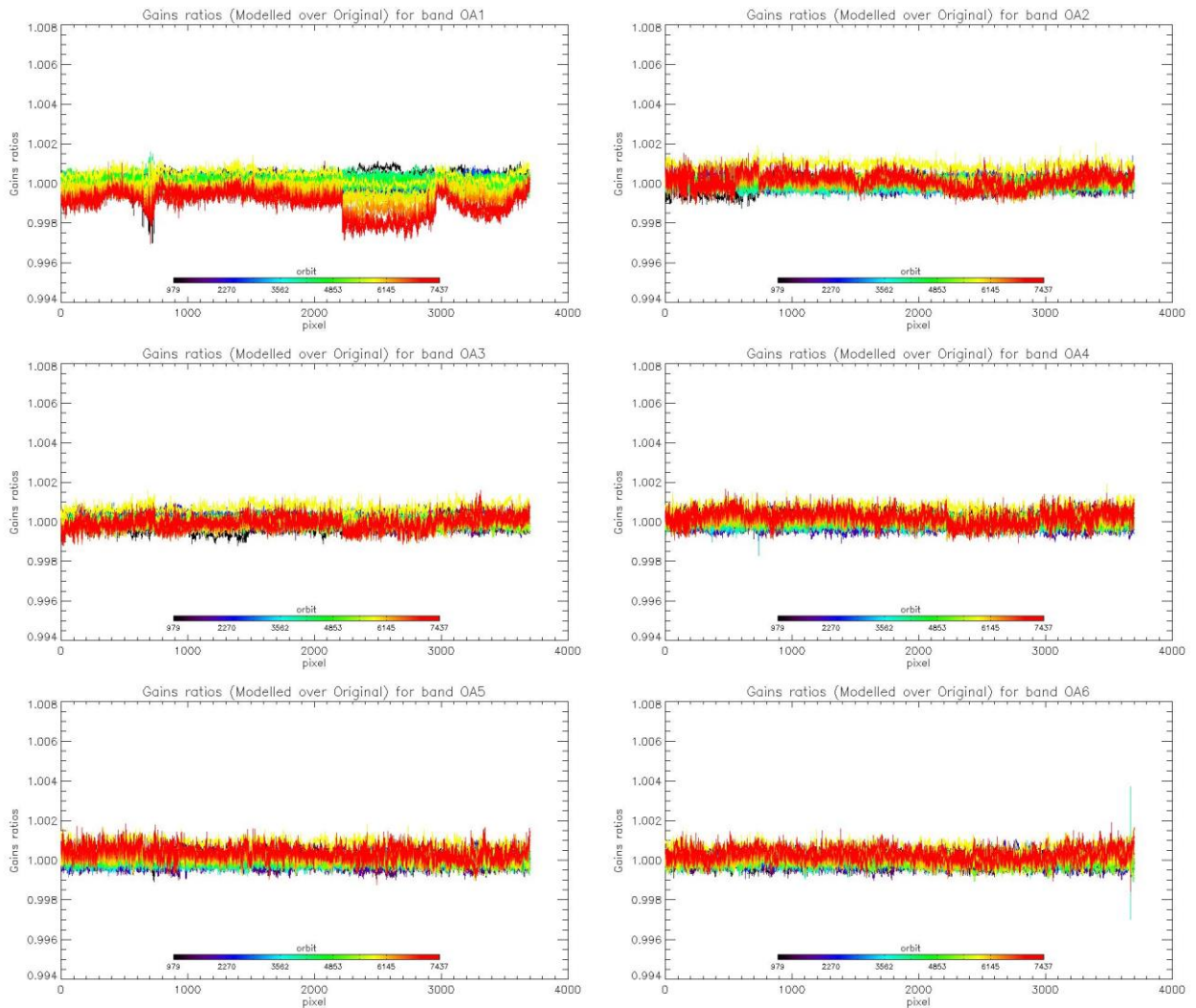


Figure 14: Evolution model performance, as ratio of Model over Data vs. pixels, all cameras side by side, over the whole current calibration dataset (since instrument programming update), including 8 calibration in extrapolation, channels Oa1 to Oa6.



Sentinel-3 MPC
S3-A OLCI Cyclic Performance Report
Cycle No. 020

Ref.: S3MPC.ACR.PR.01-020
Issue: 1.0
Date: 25/08/2017
Page: 13

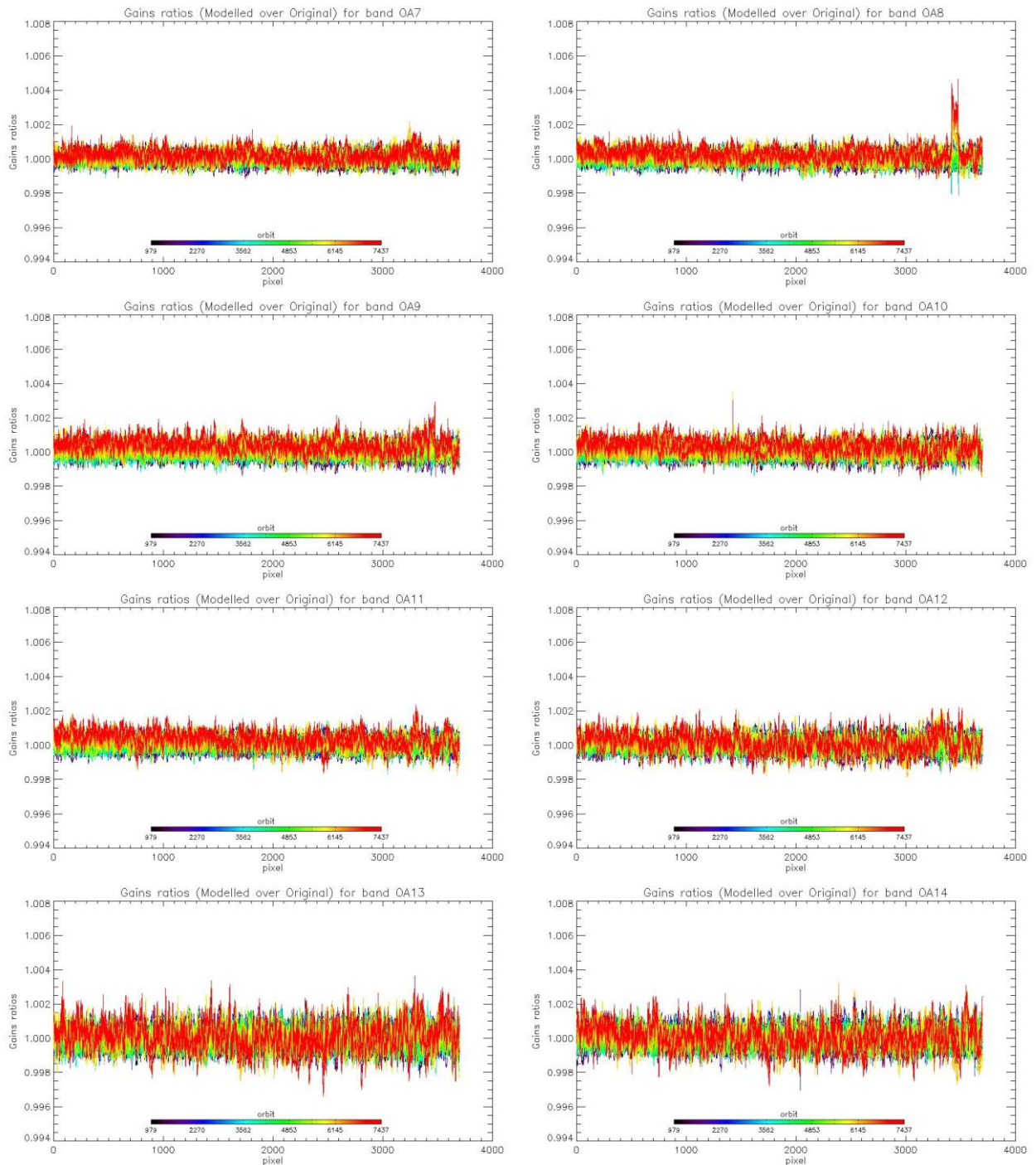


Figure 15: same as Figure 14 for channels Oa7 to Oa14.



Sentinel-3 MPC
S3-A OLCI Cyclic Performance Report
Cycle No. 020

Ref.: S3MPC.ACR.PR.01-020
 Issue: 1.0
 Date: 25/08/2017
 Page: 14

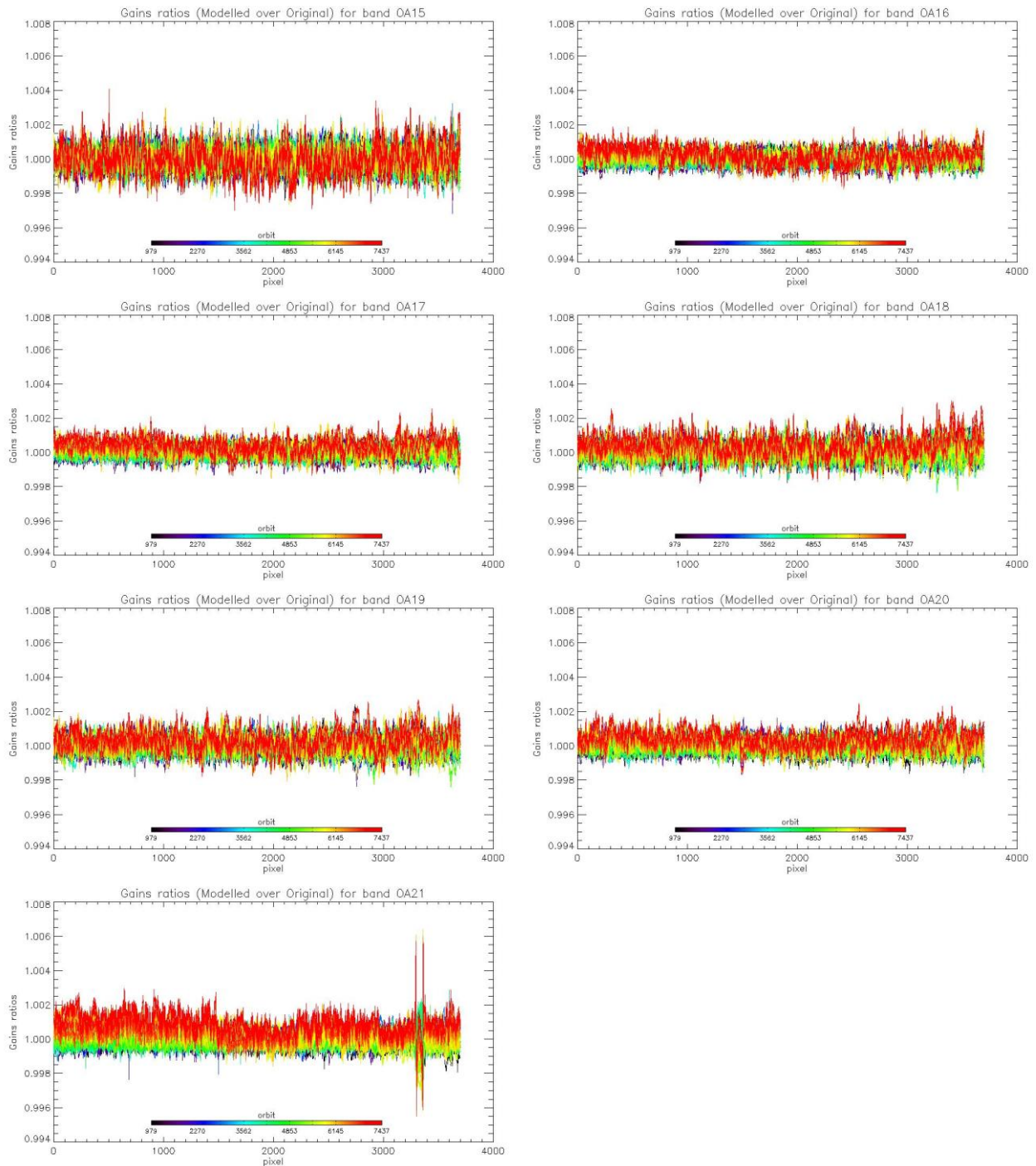


Figure 16: same as Figure 14 for channels Oa15 to Oa21.

1.2.3 Ageing of nominal diffuser [OLCI-L1B-CV-240]

There has been one calibration sequence S05 (reference diffuser) acquisition during cycle 020:

- ❖ S05 sequence (diffuser 2) on 22/07/2017 09:50 to 09:52 (absolute orbit 7438)



The diffuser 1 Ageing is computed for each 3700 detector and each spectral band by formula:

$$\text{Ageing}(\text{orb}) = G1(\text{orb})/G2(\text{orb}) - G1(\text{orb_ref})/G2(\text{orb_ref})$$

Where:

- ❖ G1 is the diffuser 1 (= nominal diffuser) Gain coefficients.
- ❖ G2 is the diffuser 2 (= reference diffuser) Gain coefficients
- ❖ orb_ref is a reference orbit chosen at the beginning of the mission

Ageing is represented in Figure 17 for band Oa1 and in Figure 18 for band Oa16. The negative shift of the sequence at orbit 5832 (for which a slight increase would be expected instead) is not explained so far and still under investigation. It should be noted that the corresponding orbit of diffuser 1 (nominal) has also been detected as an outlier in the modelling of the radiometric long-term trend (see section 1.2.2.2) with an unexpected excess of brightness.

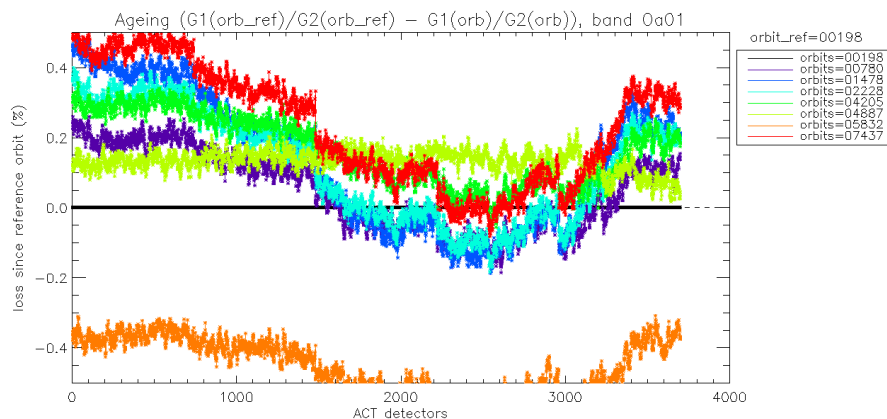


Figure 17: diffuser 1 ageing for spectral band Oa01. We see strong ACT low frequency structures that are due to residual of BRDF modelling.

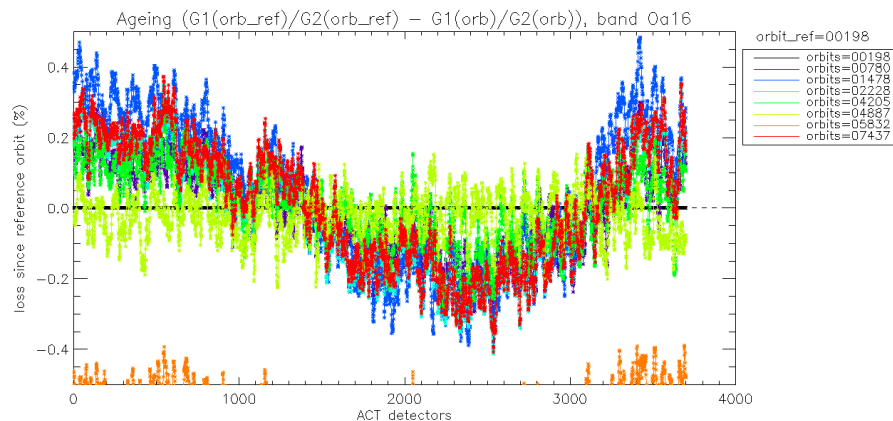


Figure 18: same as Figure 17 for spectral band Oa16. We use this band in order to normalize other bands and remove the ACT structures due to residual of BRDF modelling. Normalized curve for spectral band Oa01 is presented in Figure 19.

Figure 17 and Figure 18 show that the Ageing curves are impacted by a strong ACT pattern which is due to residuals of the bad modelling (on-ground) of the diffuser BRDF. This pattern is dependant of the azimuth angle. It is a 'white' pattern which means it is the same for all spectral bands. As such, we can remove this pattern by normalizing the ageing of all bands by the curve of band Oa16 which is expected not to be impacted by ageing because in the red part of the spectrum. We use an ACT smoothed version (window of 100 detectors) of band Oa16 in order to reduce the high frequency noise. Normalized ageing for spectral band Oa01 is represented in Figure 19 where we can see that this band is impacted by ageing of the diffuser.

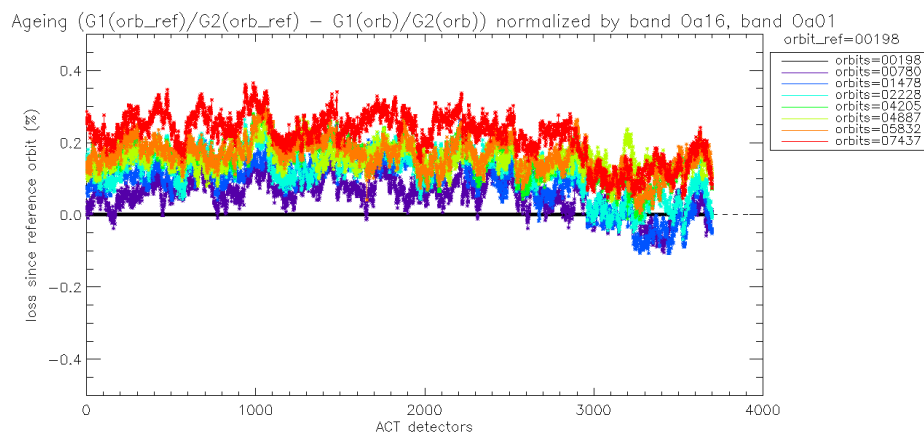


Figure 19: same as Figure 17 after normalization by band Oa16. Ageing of the diffuser 1 is now visible in the 5 cameras.

Camera averaged ageing (normalized by band Oa16) as a function of wavelength is represented in Figure 20 where we can see that ageing is stronger in the 'bluest' spectral bands (short wavelengths). Ageing is visible only for the 5 first spectral bands so far in the OLCI mission life.

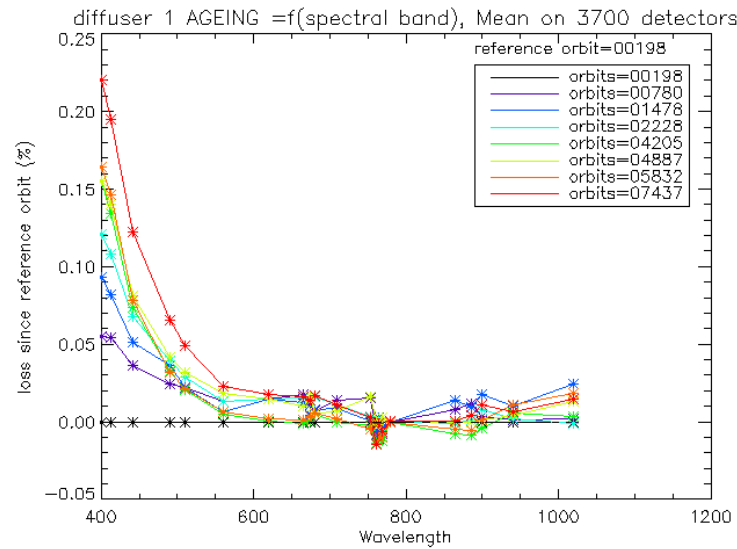


Figure 20: Diffuser 1 ageing as a function of wavelength (or spectral band). Ageing is visible in spectral band #1 to #5.

Erreur ! Source du renvoi introuvable. shows the evolution of the 5 camera averaged ageing as a function of time.

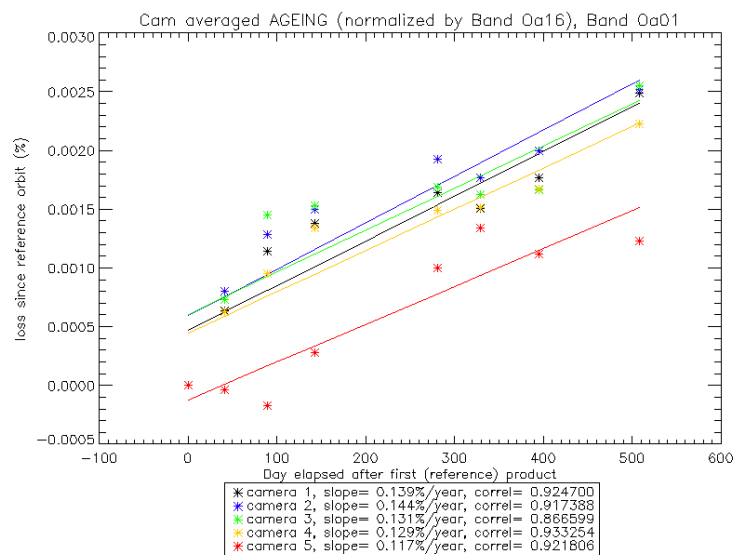


Figure 21: Camera averaged ageing (normalized by band Oa16) as a function of time. Linear fit for each camera is plotted. The slope (% loss per year) and the correlation coefficient

1.2.4 Updating of calibration ADF [OLCI-L1B-CV-260]

There has been no OL_1_CAL_AX generated during cycle 020.

	Sentinel-3 MPC S3-A OLCI Cyclic Performance Report Cycle No. 020	Ref.: S3MPC.ACR.PR.01-020 Issue: 1.0 Date: 25/08/2017 Page: 18
--	---	---

1.2.5 Radiometric Calibrations for sun azimuth angle dependency and Yaw Manoeuvres for Solar Diffuser on-orbit re-characterization [OLCI-L1B-CV-270 and OLCI-L1B-CV-280]

This activity has not evolved during cycle 020 and results presented in previous report are still valid.

1.3 Spectral Calibration [OLCI-L1B-CV-400]

There has been no Spectral Calibration acquisitions sequence S02/S03 during cycle 020.

Consequently the last updated results (cycle 018) are still valid.

1.4 Signal to Noise assessment [OLCI-L1B-CV-620]

1.4.1 SNR from Radiometric calibration data.

SNR computed for all calibration data as a function of band number is presented in Figure 22.

SNR computed for all calibration data as a function of orbit number for band Oa01 (the less stable band) is presented in Figure 23.

There is no significant evolution of this parameter during the current cycle and the ESA requirement is fulfilled for all bands.



Sentinel-3 MPC
S3-A OLCI Cyclic Performance Report
Cycle No. 020

Ref.: S3MPC.ACR.PR.01-020
 Issue: 1.0
 Date: 25/08/2017
 Page: 19

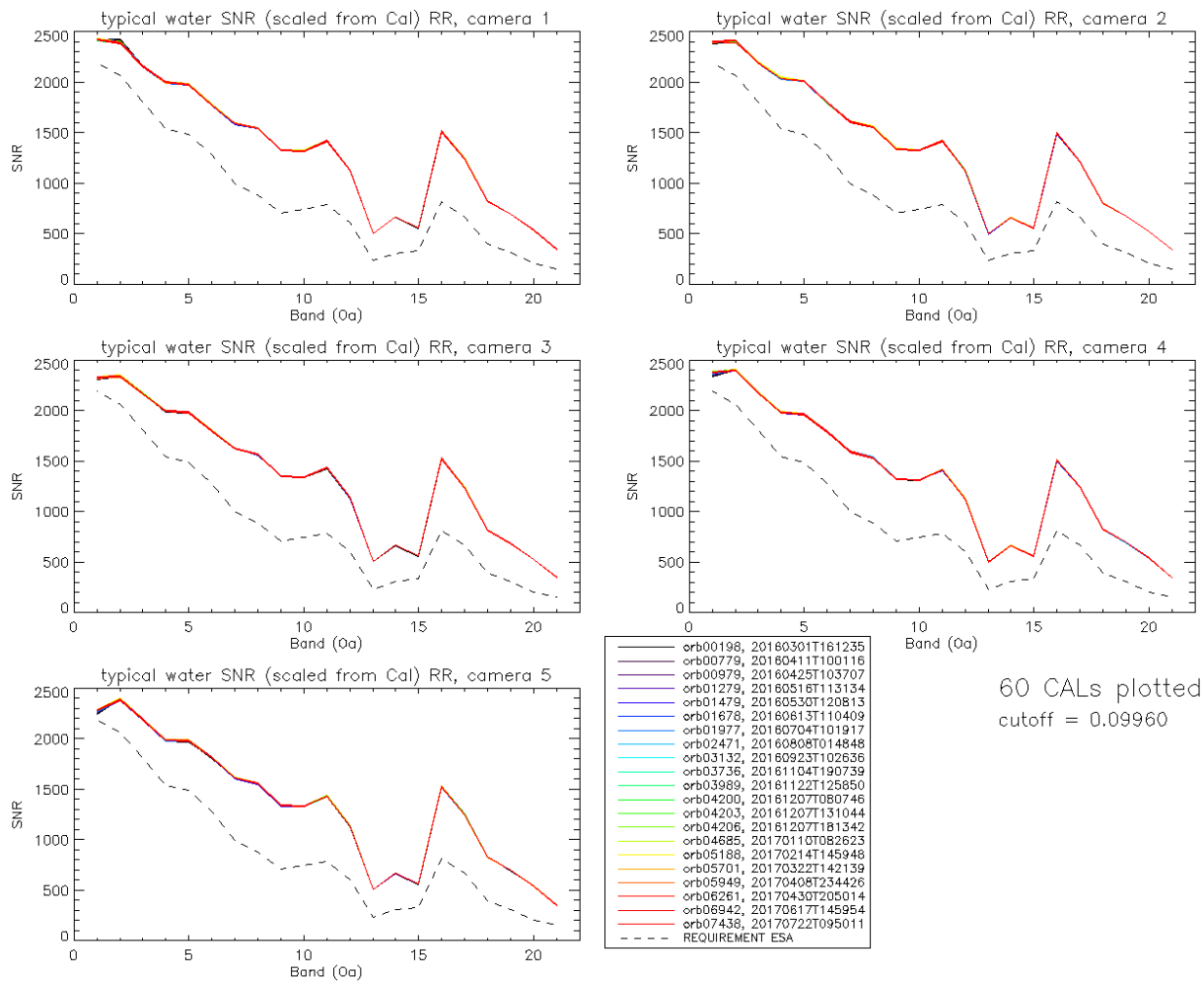


Figure 22: Signal to Noise ratio as a function of the spectral band for the 5 cameras. These results have been computed from radiometric calibration data. All calibrations except first one (orbit 183) are presents with the colours corresponding to the orbit number (see legend). The SNR is very stable with time: the curves for all orbits are almost superimposed. The dashed curve is the ESA requirement.

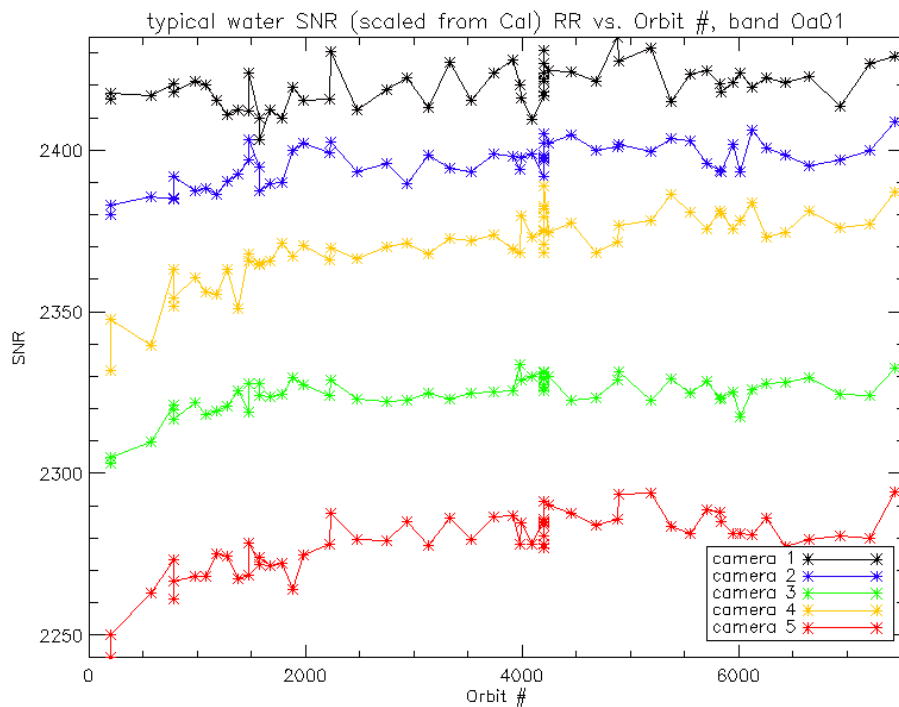


Figure 23: long-term stability of the SNR estimates from Calibration data, example of channel Oa1.

The mission averaged SNR figures are provided in Table 1 below, together with their radiance reference level. According to the OLCI SNR requirements, these figures are valid at these radiance levels and at Reduced Resolution (RR, 1.2 km). They can be scaled to other radiance levels assuming shot noise (CCD sensor noise) is the dominating term, i.e. radiometric noise can be considered Gaussian with its standard deviation varying as the square root of the signal; in other words: $SNR(L) = SNR(L_{ref}) \cdot \sqrt{\frac{L}{L_{ref}}}$. Following the same assumption, values at Full Resolution (300m) can be derived from RR ones as 4 times smaller.



Sentinel-3 MPC
S3-A OLCI Cyclic Performance Report
Cycle No. 020

Ref.: S3MPC.ACR.PR.01-020
 Issue: 1.0
 Date: 25/08/2017
 Page: 21

Table 1: SNR figures as derived from Radiometric Calibration data. Figures are given for each camera (time average and standard deviation), and for the whole instrument. The requirement and its reference radiance level are recalled (in $mW.sr^{-1}.m^{-2}.nm^{-1}$).

λ	L_{ref}	SNR	C1		C2		C3		C4		C5		All	
			avg	std	avg	std	avg	std	avg	std	avg	std	avg	std
400	63	2188	2420	6.6	2395	6.1	2324	6	2370	11.1	2278	10.2	2357	6.5
412.5	74.1	2061	2397	8.3	2409	5.4	2340	4.8	2402	4.6	2386	7.3	2387	4.2
442.5	65.6	1811	2161	5.4	2199	5.8	2167	4.4	2185	4.4	2197	4.8	2182	3.4
490	51.2	1541	1999	5.1	2035	5.4	1995	3.5	1981	4.1	1987	5.2	1999	3.6
510	44.4	1488	1979	5.5	2012	4.9	1982	4.7	1965	4.6	1984	5	1984	3.9
560	31.5	1280	1775	4.4	1801	4.5	1801	4.9	1793	4	1817	3.9	1798	3.3
620	21.1	997	1591	4.3	1609	4.2	1625	3.4	1593	3.6	1614	3.7	1606	2.8
665	16.4	883	1546	4.7	1558	4.3	1566	3.8	1532	4.4	1560	4	1552	3.3
673.75	15.7	707	1329	3.5	1338	4.1	1350	3	1323	3.1	1341	4.1	1336	2.8
681.25	15.1	745	1319	3.8	1326	3.2	1337	3.1	1314	2.5	1332	3.9	1326	2.4
708.75	12.7	785	1420	4.7	1420	4.4	1434	3.8	1413	3.9	1429	3.2	1423	3.2
753.75	10.3	605	1126	3.5	1119	3.4	1133	4	1123	2.7	1138	3	1128	2.8
761.25	6.1	232	501	1.3	498	1.5	504	1.4	500	1.2	507	1.6	502	1.1
764.375	7.1	305	662	1.8	657	1.7	667	2.5	660	1.8	668	2.1	663	1.7
767.5	7.6	330	558	1.8	554	1.4	561	1.6	556	1.8	563	1.5	558	1.4
778.75	9.2	812	1513	5.5	1495	5.4	1522	5.6	1508	5.7	1524	5.2	1513	4.8
865	6.2	666	1243	3.8	1212	4.5	1237	4.5	1245	3.9	1249	3	1237	3.4
885	6	395	823	1.9	801	1.8	813	2.1	824	1.6	830	2	818	1.4
900	4.7	308	691	1.7	673	1.4	682	1.8	692	1.5	697	1.5	687	1.1
940	2.4	203	534	1	522	1.2	525	1	539	1.2	541	1.2	532	0.8
1020	3.9	152	345	0.8	337	0.7	348	0.7	345	0.7	351	0.7	345	0.5

1.4.2 SNR from EO data.

There has been no update on SNR assessment from EO data during the cycle. Last figures (cycle 9) are considered valid.

1.5 Geometric Calibration/Validation

Regular monitoring using the GeoCal Tool implemented within the MPMF continues. Late June results confirm good performance. Monitoring of the geolocation performance by correlation with GCP imageries using the GeoCal tool over the period confirms that OLCI is compliant with its requirement: the centroid of the geolocation error is around 0.25 pixel in both along-track and across-track directions

(Figure 24: histograms of geolocation errors for the along-track (left) and across-track (right) directions, example of 25/07/2017.)

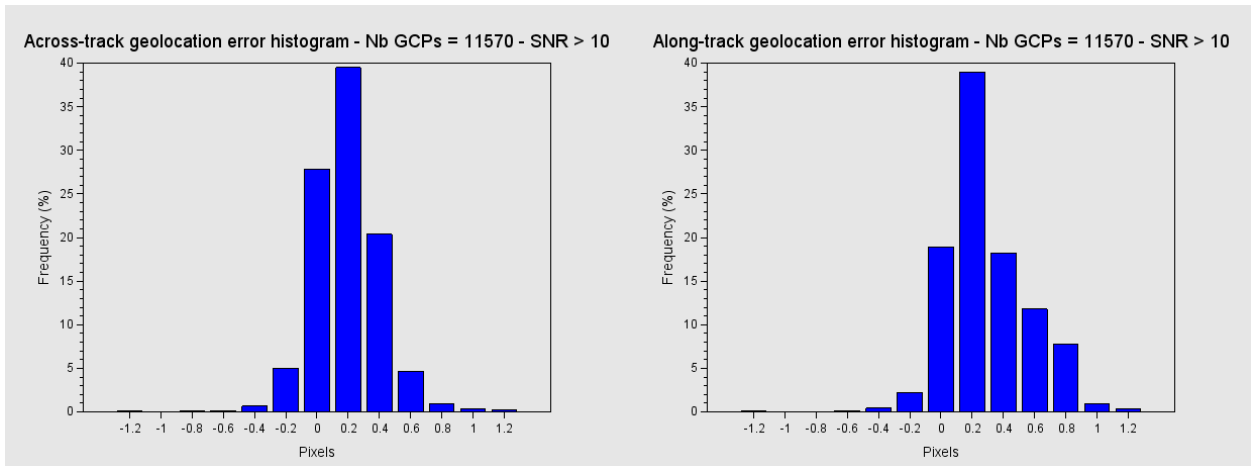


Figure 24: histograms of geolocation errors for the along-track (left) and across-track (right) directions, example of 25/07/2017.

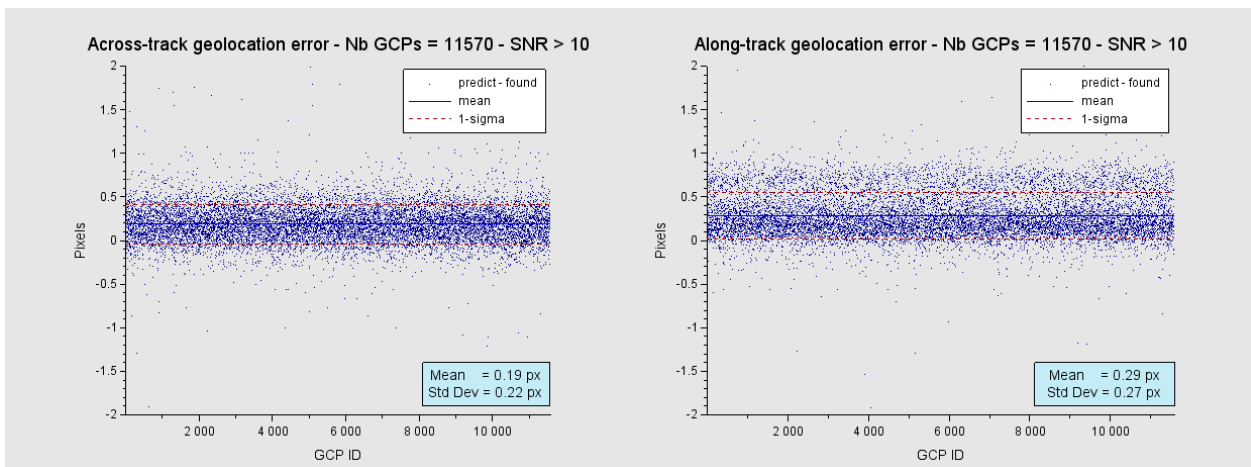


Figure 25: georeferencing error in along-track (left) and across-track (right) directions for all the GCPs.

The series plots of along-track and across-track georeferencing errors for the 25th of July 2017 (Figure 25) confirm the good overall performance of the geometric calibration. Statistics are derived after filtering on correlation quality (thresholding on the so-called “SNR” reported on the figures) as well as on the error magnitude itself as some ambiguous cases remain (errors higher than 5 pixels are excluded, as never confirmed by visual analysis of scenes). Note that the second filtering was introduced in after about two months of monitoring and proved to have no or very low impact on the averages while it significantly decreases the standard deviations (Figure 26): values for May and June 2017 were obtained without while earlier (reprocessed data, May 2016 to March 2107, 1 day per month) and more recent



Sentinel-3 MPC
S3-A OLCI Cyclic Performance Report
Cycle No. 020

Ref.: S3MPC.ACR.PR.01-020
 Issue: 1.0
 Date: 25/08/2017
 Page: 23

data (July and early August 2017) were analysed including the thresholding on the errors magnitude, explaining the large increase of dispersion values in May and June 2017.

The long term time series (Figure 26) highlight a small but continuous trend in AL average that does not seem to be cyclic and a slight discrete increase of the across-track average error in November 2016. In-depth analysis, in particular regarding camera and pixel dependencies, as well as potential latitudinal effects, is on-going.

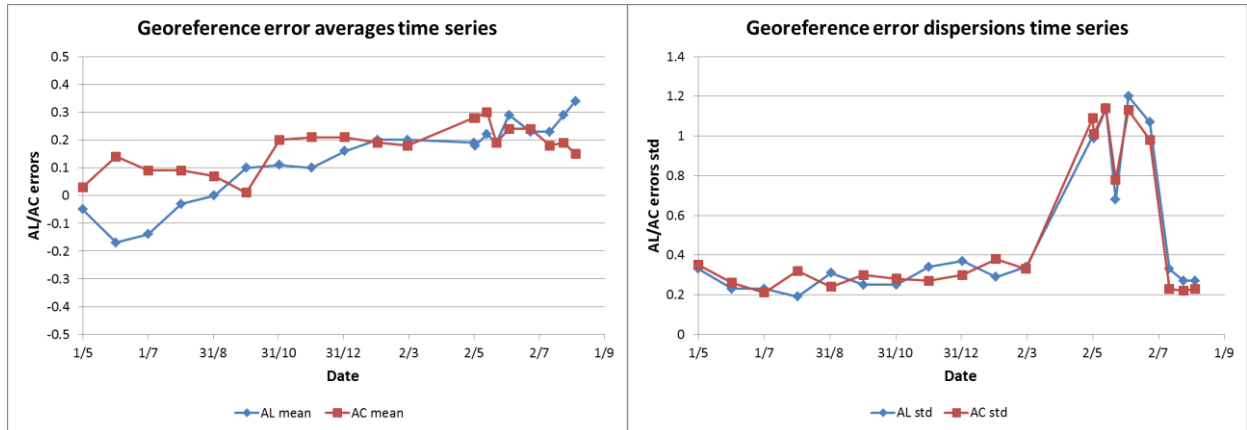


Figure 26: average and dispersion time series of the geolocation errors in along-track (blue) and across-track (red) directions over 15 months.

	Sentinel-3 MPC S3-A OLCI Cyclic Performance Report Cycle No. 020	Ref.: S3MPC.ACR.PR.01-020 Issue: 1.0 Date: 25/08/2017 Page: 24
--	---	---

2 OLCI Level 1 Product validation

2.1 [OLCI-L1B-CV-300], [OLCI-L1B-CV-310] – Radiometric Validation

2.1.1 S3ETRAC Service

Activities done

The S3ETRAC service extracts OLCI L1 RR and SLSTR L1 RBT data and computes associated statistics over 49 sites corresponding to different surface types (desert, snow, ocean maximizing Rayleigh signal, ocean maximizing sunglint scattering and deep convective clouds). The S3ETRAC products are used for the assessment and monitoring of the L1 radiometry (optical channels) by the ESLs.

All details about the S3ETRAC/OLCI and S3ETRAC/SLSTR statistics are provided on the S3ETRAC website <http://s3etrac.acri.fr/index.php?action=generalstatistics>

- ❖ Number of OLCI products processed by the S3ETRAC service
- ❖ Statistics per type of target (DESERT, SNOW, RAYLEIGH, SUNGLINT and DCC)
- ❖ Statistics per sites
- ❖ Statistics on the number of records

For illustration, we provide below statistics on the number of S3ETRAC/OLCI records generated per type of targets (DESERT, SNOW, RAYLEIGH, SUNGLINT and DCC).

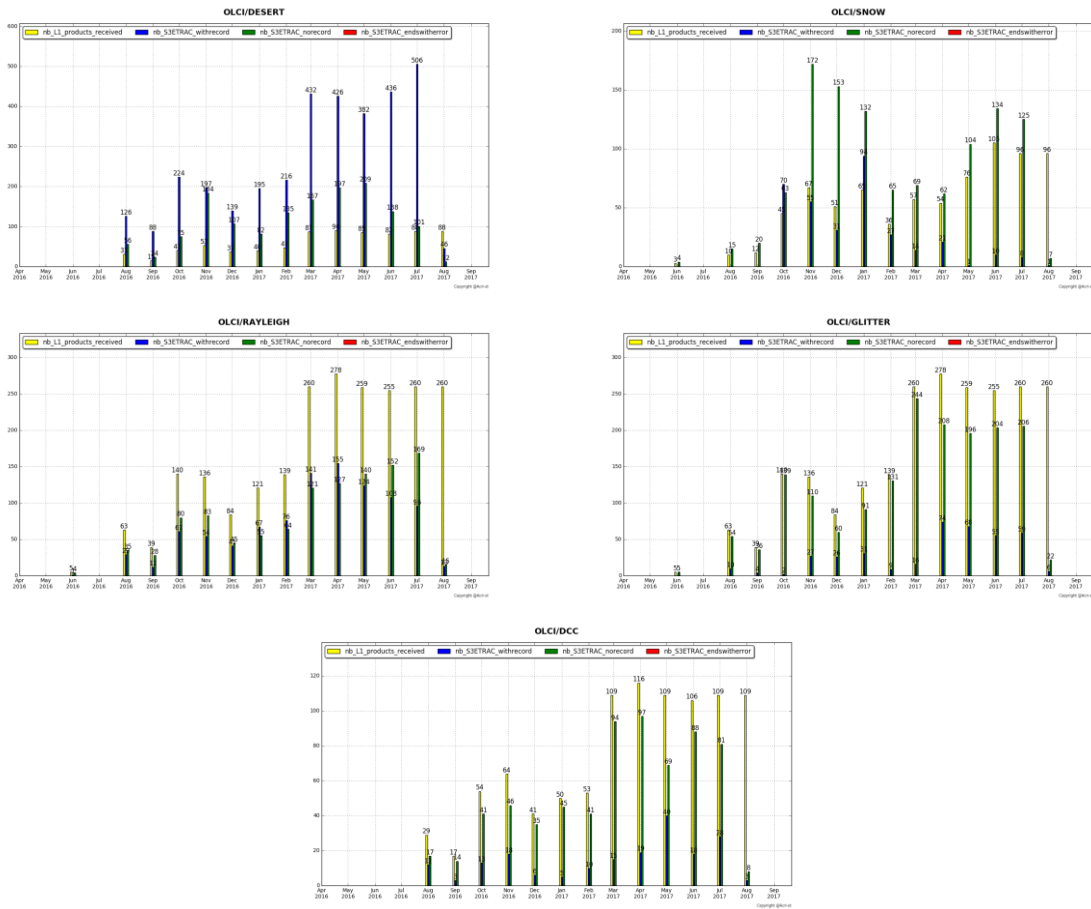


Figure 27: summary of S3ETRAC products generation for OLCI (number of OLCI L1 products Ingested, yellow – number of S3ETRAC extracted products generated, blue – number of S3ETRAC runs without generation of output product (data not meeting selection requirements), green – number of runs ending in error, red, one plot per site type).

2.1.2 Radiometric validation with DIMITRI

Highlights

- ❖ Run Desert and Rayleigh method over the available products until 18th August.
- ❖ The results are consistent with the previous ones (Rayleigh, Glint and PICS).
- ❖ Rather good stability of the sensor could be seen, nevertheless, the time-series average shows higher reflectance over the VNIR spectral range with bias of 3%-5% except bands Oa07-Oa09; bands with high gaseous absorption are excluded.
- ❖ The results are consistent over the used CalVal sites
- ❖ The results need to be consolidated over ocean sites with more products from early mission period.

	<p>Sentinel-3 MPC</p> <p>S3-A OLCI Cyclic Performance Report</p> <p>Cycle No. 020</p>	<p>Ref.: S3MPC.ACR.PR.01-020</p> <p>Issue: 1.0</p> <p>Date: 25/08/2017</p> <p>Page: 26</p>
--	--	--

I-Validation over PICS

1. Downloading and ingestion of all the available L1B-LN1-NT products in the S3A-Opt database over the 6 desert calval-sites (Algeria3 & 5, Libya 1 & 4 and Mauritania 1 & 2) is on-going. The ingested time-series has been extended until 15th August 2017. Note that only few products over the 6 PICS were found during Cycle-20 period due to an issue with the mini-file generation.
2. The results are consistent overall the six used PICS sites (Figure 28). OLCI reflectance shows rather good stability over the mission life-time.
3. The temporal average over the period **April 2016 – August 2017** of the elementary ratios (observed reflectance to the simulated one) shows values higher than 2% (mission requirements) over all the VNIR bands (Figure 29). The spectral bands with significant absorption from water vapour and O₂ (Oa11, Oa13 and Oa14) show an outlier ratio.

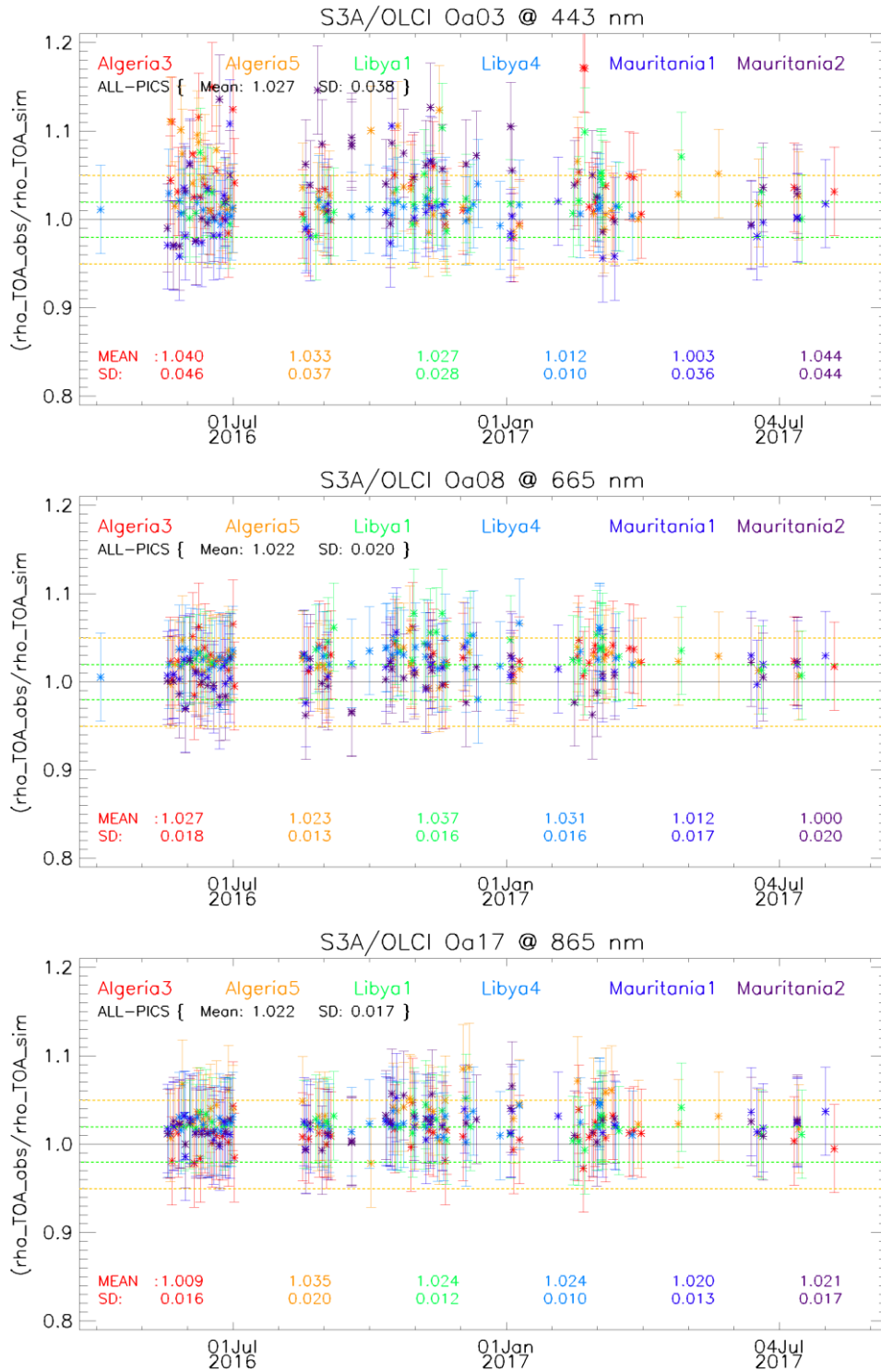


Figure 28: Time-series of the elementary ratios (observed/simulated) signal from S3A/OLCI for (top to bottom) bands Oa03, Oa08 and Oa17 respectively over Six PICS Cal/Val sites. Dashed-green and orange lines indicate the 2% and 5% respectively. Error bars indicate the desert methodology uncertainty.

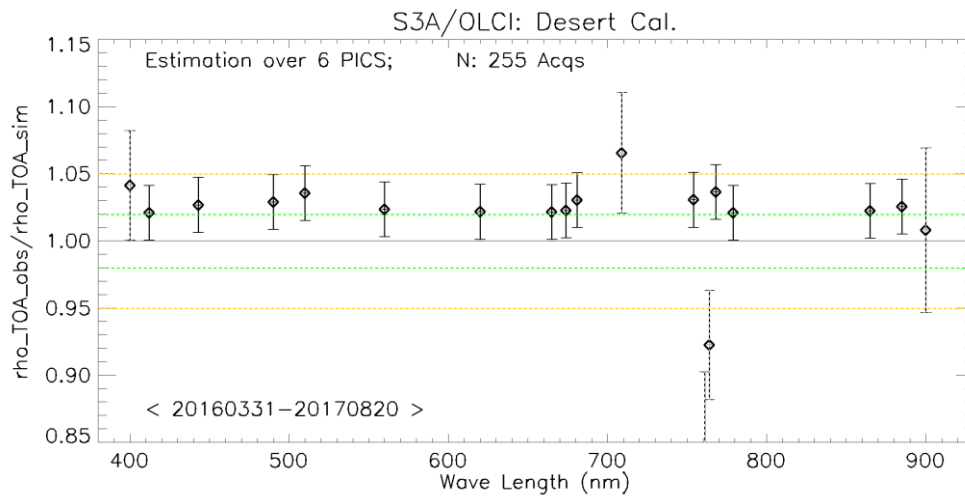


Figure 29: The estimated gain values for S3A/OLCI over the 6 PICS sites identified by CEOS over the period April 2016 – July 2017 as a function of wavelength. Dashed-green and orange lines indicate the 2% and 5% respectively. Error bars indicate the desert methodology uncertainty.

II-Intercomparison S3A/OLCI, S2A/MSI and LANDSAT/OLI over PICS

1. X-mission Intercomparison with MSI-A and MODIS-A is performed until August 2017. Figure 30 shows time-series of the elementary ratios from S2A/MSI, Aqua/MODIS and S3A/OLCI over ALGERIA5 and LIBYA1 over the period March-2016 until August-2017.

We observe a clear stability over the three sensors, associated with high reflectance from OLCI wrt to MSI and MODIS ones.

Figure 31 shows the estimated gain over the time-series from Figure 30 for the common bands between S2A/MSI, Aqua/MODIS and S3A/OLCI over ALGERIA5 and LIBYA1. Again Figure 31 confirms a systematic higher reflectance of OLCI wrt MSI and MODISA.

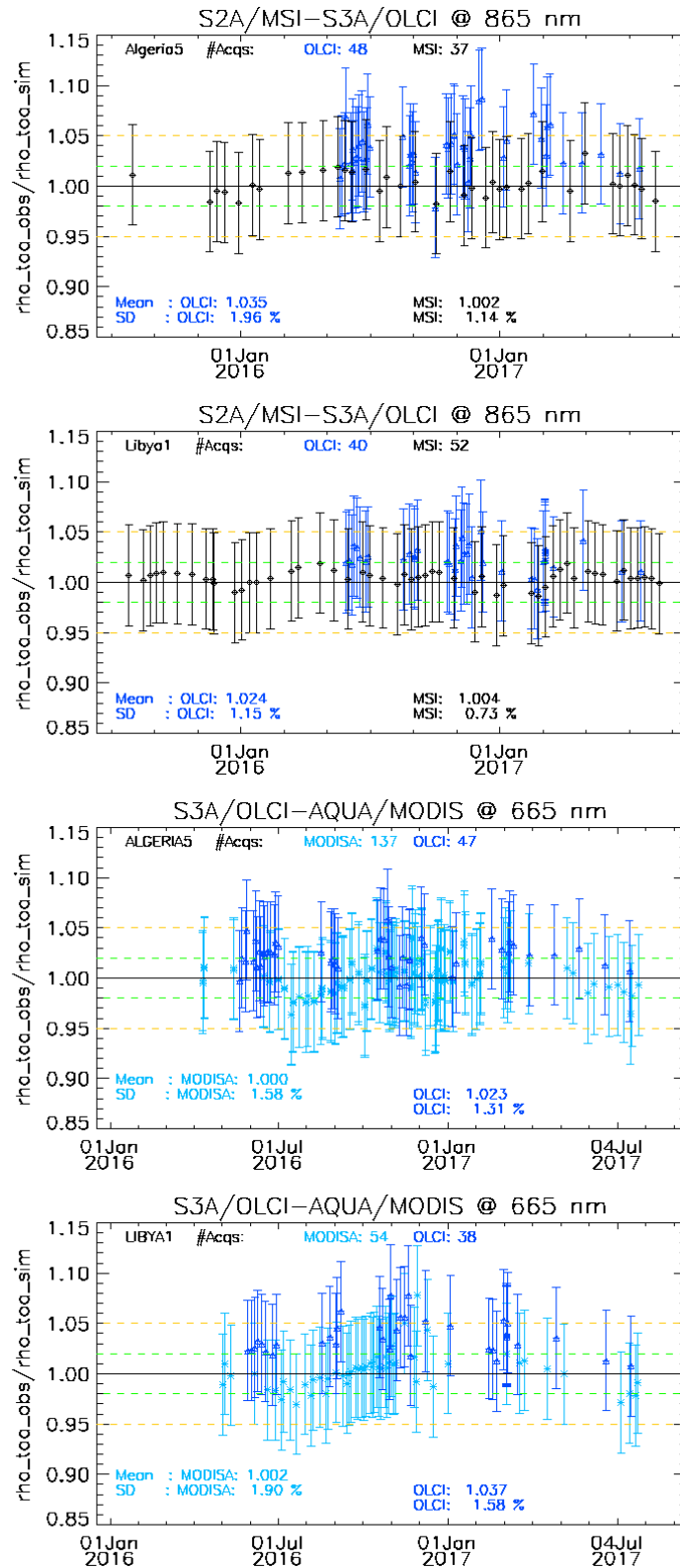


Figure 30: Time-series of the elementary ratios (observed/simulated) signal from (black) S2A/MSI, (blue) S3A/OLCI and (Cyan) Aqua/MODIS for (band Oa17: 865nm and Oa08: 665 nm over ALGERIA5 and LIBYA1 sites. Dashed-green and orange lines indicate the 2% and 5% respectively. Error bars indicate the desert methodology uncertainty.

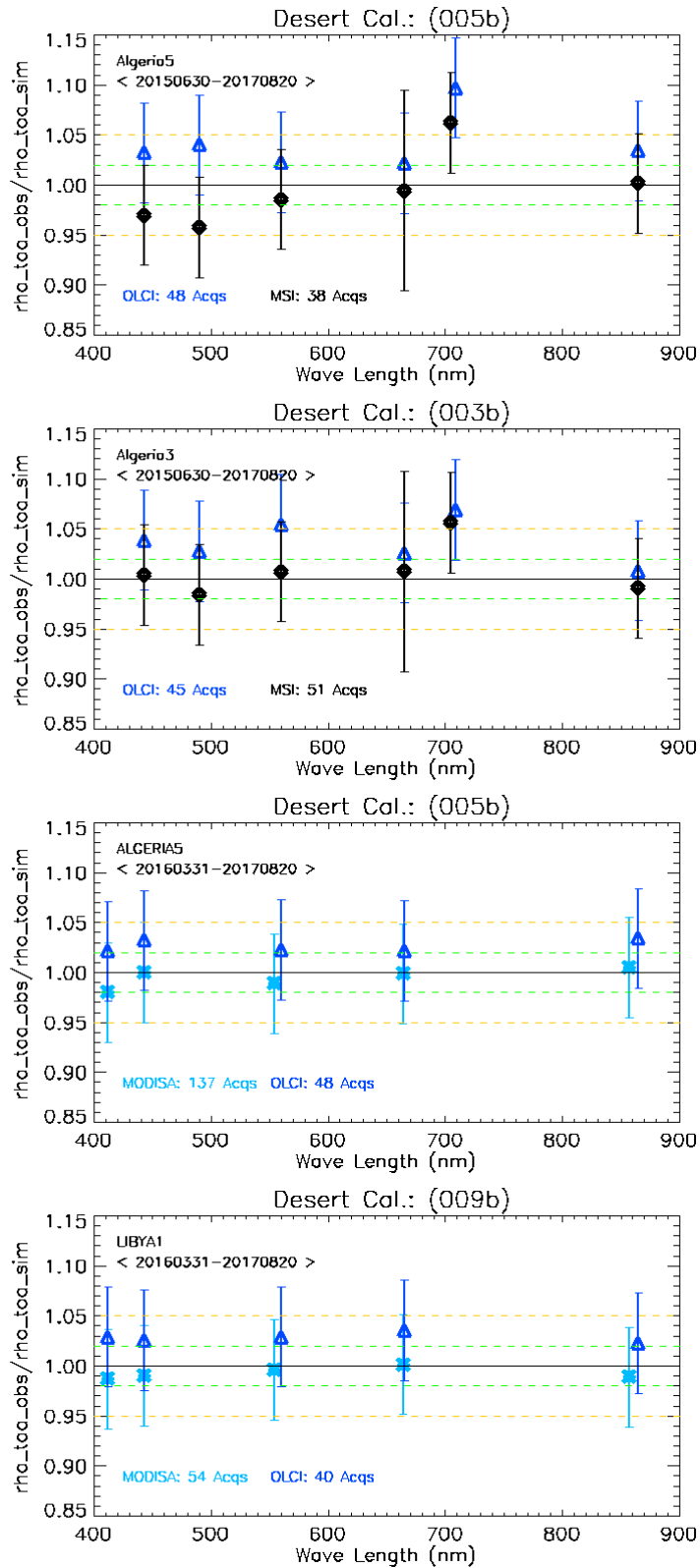


Figure 31: The estimated gain values (observed-signal / simulated-signal) averaged over the period April-August 2017 from (black)S2A/MSI, (blue) S3A/OLCI and (Cyan) Aqua/MODIS over ALGERIA5 and LIBYA1 sites as function of wavelength. Dashed-green and orange lines indicate the 2% and 5% respectively. Error bars indicate the desert methodology uncertainty.



III-Validation over Rayleigh

Rayleigh method has been performed over the available mini-files on the Opt-server over the cycle-20 period. The results produced with the configuration (ROI-AVERAGE) are consistent with the previous results of PICS method and from Cycle-19. While bands Oa01-Oa05 display a bias values between 2%-5%, bands Oa6-Oa9 exhibit biases within 2% (mission requirements) (Figure 32).

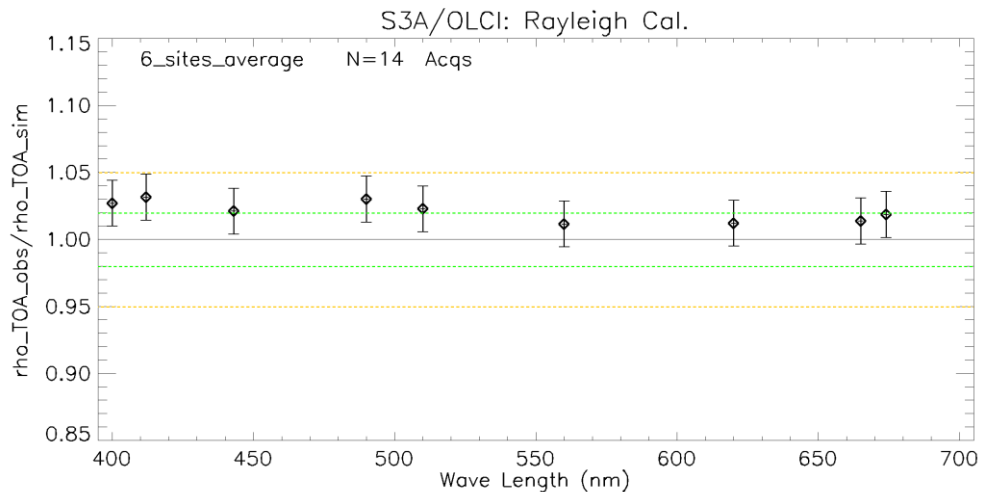


Figure 32: The estimated gain values for S3A/OLCI over the 6 Ocean CalVal sites (Atl-NW_Optimum, Atl-SW_Optimum, Pac-NE_Optimum, Pac-NW_Optimum, SPG_Optimum and SIO_Optimum) over the period December 2016 – August 2017 as a function of wavelength. Dashed-green, and orange lines indicate the 2%, 5% respectively. Error bars indicate the methodology uncertainty.

IV-Validation over Glint

There has been no new Glint method result during the cycle. Last figures (cycle 19) are considered valid.

2.1.3 Radiometric validation with OSCAR

There has been no new OSCAR result during the cycle. Last figures (cycle 19) are considered valid.

	<p>Sentinel-3 MPC</p> <p>S3-A OLCI Cyclic Performance Report</p> <p>Cycle No. 020</p>	<p>Ref.: S3MPC.ACR.PR.01-020</p> <p>Issue: 1.0</p> <p>Date: 25/08/2017</p> <p>Page: 32</p>
--	--	--

2.2 [OLCI-L1B-CV-320] – Radiometric Validation with Level 3 products

Summary of activities

A method to estimate the product biases at high latitudes has been applied to OLCI data processed with Polymer and the standard atmospheric correction algorithm. This method shows a strong over-estimation of the water reflectances from the standard product in high air mass conditions. The OLCI Polymer product shows a very good consistency, in high air mass conditions, better than for MERIS, suggesting that the radiometry is not the source of discrepancies.

Description of activities done and results

OLCI consistency at high latitudes

A method previously applied to MERIS, MODIS and SeaWiFS (see e.g. the poster presented at IOCS 2015 [here](#)) has been applied to OLCI data, processed both with Polymer and with the standard atmospheric correction. This method consists in comparing the water reflectances from a given product, between multiple orbits in the same day, in the Arctic region, close to the summer solstice. These multiple daily observations are realized under variable geometries, in particular with highly variable sun zenith angles, which allows estimating the influence of the air mass on the retrieved reflectances:

- ❖ Each ocean point in the Arctic and in summer can be observed several times per day due to overlapping orbits (see Figure 33).
- ❖ Time difference is less than 12 hours; natural variations of the ocean reflectance can be neglected
- ❖ Water reflectances are fully normalized, thus should be independent of the observation geometry
- ❖ Analysis performed in terms of air mass, $m^* = 1/\cos(\text{sza}) + 1/\cos(\text{vza})$
- ❖ This allows assessing the bias at high latitudes without requiring in-situ data

	<p>Sentinel-3 MPC</p> <p>S3-A OLCI Cyclic Performance Report</p> <p>Cycle No. 020</p>	<p>Ref.: S3MPC.ACR.PR.01-020</p> <p>Issue: 1.0</p> <p>Date: 25/08/2017</p> <p>Page: 33</p>
--	--	--

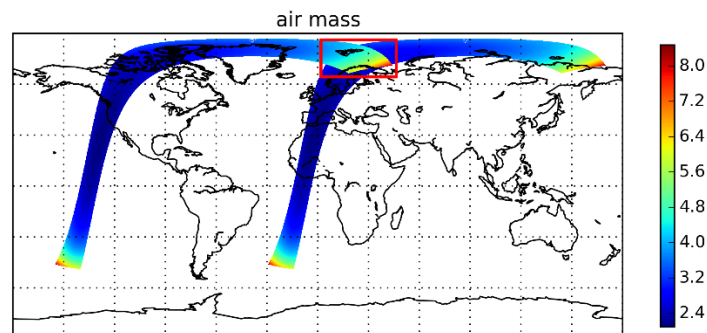


Figure 33: Illustration of the comparison of the water reflectances retrieved under various geometry conditions (air mass) in the same day, in the Arctic region.

The following software and flag configurations have been used:

OLCI L1 and L2 from S3MPC ftp server (as of late June, 2017)

- ❖ Acquisition date June 10 to 20, 2017
- ❖ MERIS data for June 1-9, 2010

Polymer:

- ❖ Polymer v4.2
- ❖ Flags applied: CLOUD (Polymer), INVALID, NEGATIVE_BB, OUT_OF_BOUNDS, EXCEPTION, THICK_AEROSOLS
- ❖ Not applied: HIGH_AIR_MASS

OLCI standard:

- ❖ IPF 06.09
- ❖ Flags applied: INVALID, LAND, CLOUD, SNOW_ICE, INLAND_WATER, TIDAL, COSMETIC, SUSPECT, SATURATED, MEDGLINT, HIGHGLINT, WHITECAPS, ADJAC, AC_FAIL, BPAC_ON, WHITE_SCATT, LOWRW, HIGHRW
- ❖ Not applied: HISOLZEN

Results

Figure 34 shows the results of the self-consistency comparison for the parameter Rw412. The slope of the linear regression indicates the impact of the air mass on the bias. We can see a strong impact of the air mass, thus sun zenith angle, on the reflectance at 412 for the standard OLCI product. The impact on the Polymer OLCI product is minor, thus it is likely that a problem affects the standard L2 product, rather than a sensor problem. For MERIS, previous results have shown relatively close results for MERIS processed by both algorithms.



Figure 35 summarises the self-consistency slopes for all bands, and confirms that the effect observed at 412 nm affects all bands, with decreasing intensity towards the red bands, as is commonly observed.

This analysis will be repeated with updated OLCI standard Level2 products, and also with MERIS products from the 4th reprocessing.

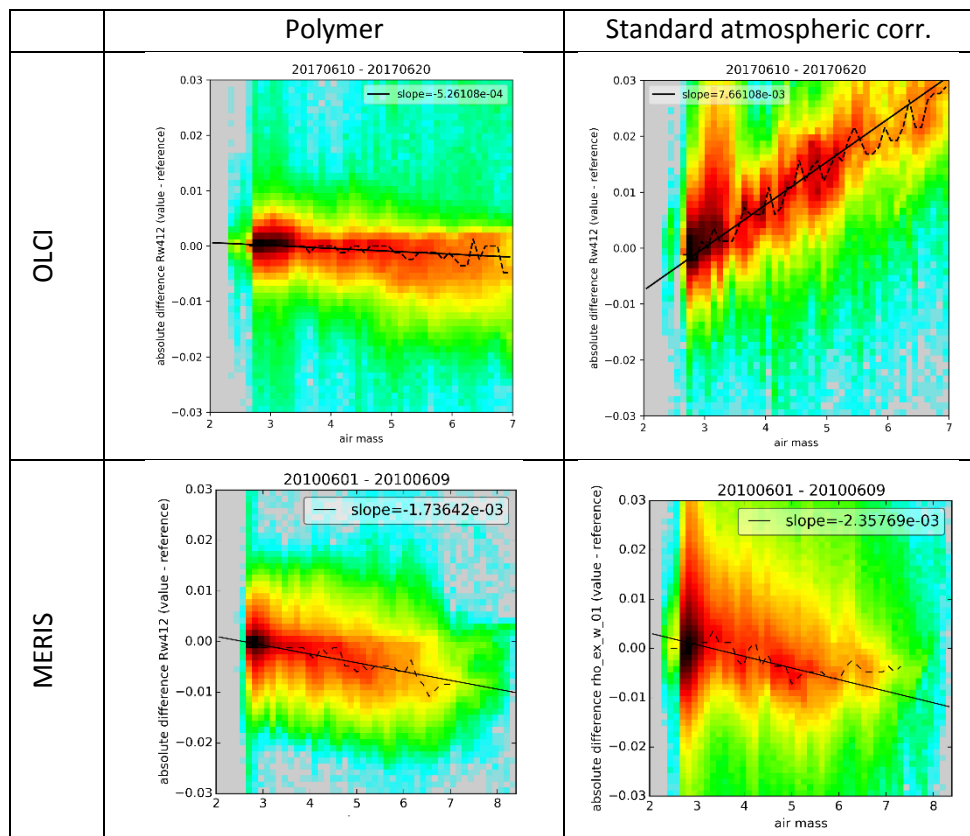


Figure 34: self-consistency results of OLCI and MERIS Rw412 products. Each plot shows the variation of the water reflectance with the reference observation (the observation at minimal air mass) from the same day. The slope of the fit gives the dependency of Rw412 on the air mass.

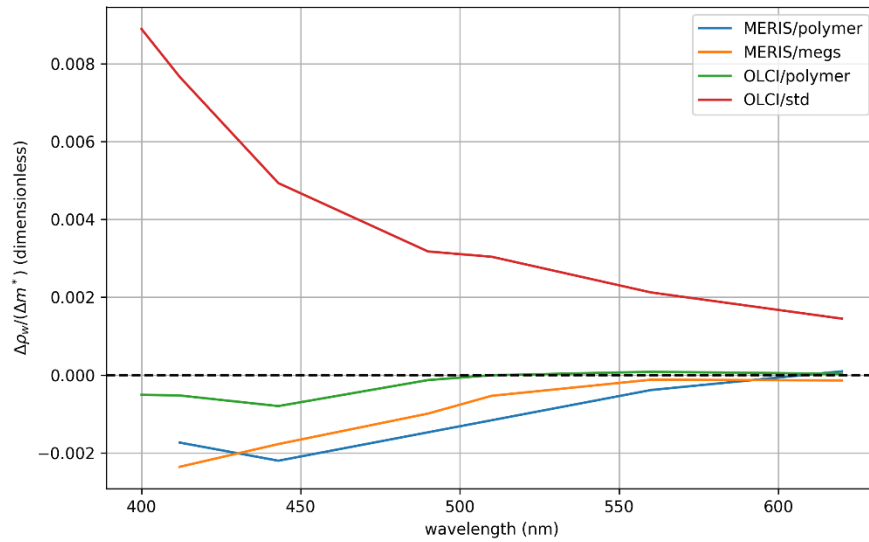


Figure 35: Summary of the self-consistency slopes (see previous figure) for each band, and for each product.



3 Level 2 Land products validation

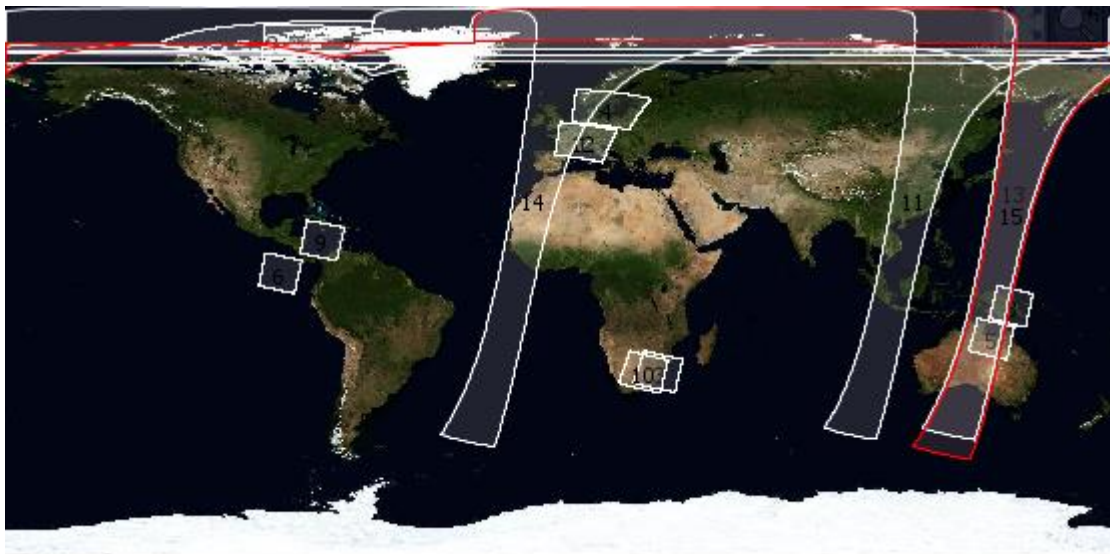
3.1 [OLCI-L2LRF-CV-300]

There has been no update on Land products validation quantitative assessment during the cycle. Last figures (cycle 18) are considered valid.

Qualitative assessment by product inspection showed no detectable performance evolution.

3.2 [OLCI-L2LRF-CV-410 & OLCI-L2LRF-CV-420] – Cloud Masking & Surface Classification for Land Products

After the change in the PDGS baseline and public release on 5.7.2017, 14 level 2 products were analysed for cloud mask quality during this cycle. This analysis includes 10 FR and 4 RR products.



Analyzed products
S3A_OL_2_LFR___20170706T093228_20170706T093528_20170707T141517_0179_019_307_1980_LN1_O_NT_002.SEN3
S3A_OL_2_LFR___20170707T021031_20170707T021321_20170708T070030_0169_019_317_1270_LN1_O_NT_002.SEN3
S3A_OL_2_LFR___20170708T072307_20170708T072607_20170708T091358_0179_019_334_3420_SVL_O_NR_002.SEN3
S3A_OL_2_LFR___20170717T095026_20170717T095326_20170717T120005_0179_020_079_2159_SVL_O_NR_002.SEN3
S3A_OL_2_LFR___20170719T155401_20170719T155701_20170719T174256_0179_020_111_2880_SVL_O_NR_002.SEN3
S3A_OL_2_LFR___20170724T002113_20170724T002413_20170725T053257_0179_020_173_3239_LN1_O_NT_002.SEN3
S3A_OL_2_LFR___20170725T161754_20170725T162054_20170726T212822_0179_020_197_1619_LN1_O_NT_002.SEN3
S3A_OL_2_LFR___20170809T000315_20170809T000615_20170809T015230_0179_021_016_3059_SVL_O_NR_002.SEN3
S3A_OL_2_LFR___20170811T074150_20170811T074450_20170811T092427_0179_021_049_3420_SVL_O_NR_002.SEN3
S3A_OL_2_LFR___20170813T095026_20170813T095326_20170814T134415_0179_021_079_2160_LN1_O_NT_002.SEN3



Sentinel-3 MPC

S3-A OLCI Cyclic Performance Report

Cycle No. 020

Ref.: S3MPC.ACR.PR.01-020

Issue: 1.0

Date: 25/08/2017

Page: 37

S3A_OL_2_LRR____20170707T021031_20170707T025341_20170708T064049_2589_019_317_____LN1_O_NT_002.SEN3
S3A_OL_2_LRR____20170708T000211_20170708T004632_20170709T043245_2661_019_330_____LN1_O_NT_002.SEN3
S3A_OL_2_LRR____20170723T102001_20170723T110419_20170724T140254_2658_020_165_____LN1_O_NT_002.SEN3
S3A_OL_2_LRR____20170808T000018_20170808T004433_20170809T050312_2655_021_002_____LN1_O_NT_002.SEN3

For the analysis pairs of level 1 (L1) and level 2 (L2) products were downloaded from the Copernicus open access hub (<https://scihub.copernicus.eu/>). Using SNAP, the cloud and snow flags were then transferred from the L2 to the L1 product. This procedure allows to view the flags over an RGB image using the original radiances values.

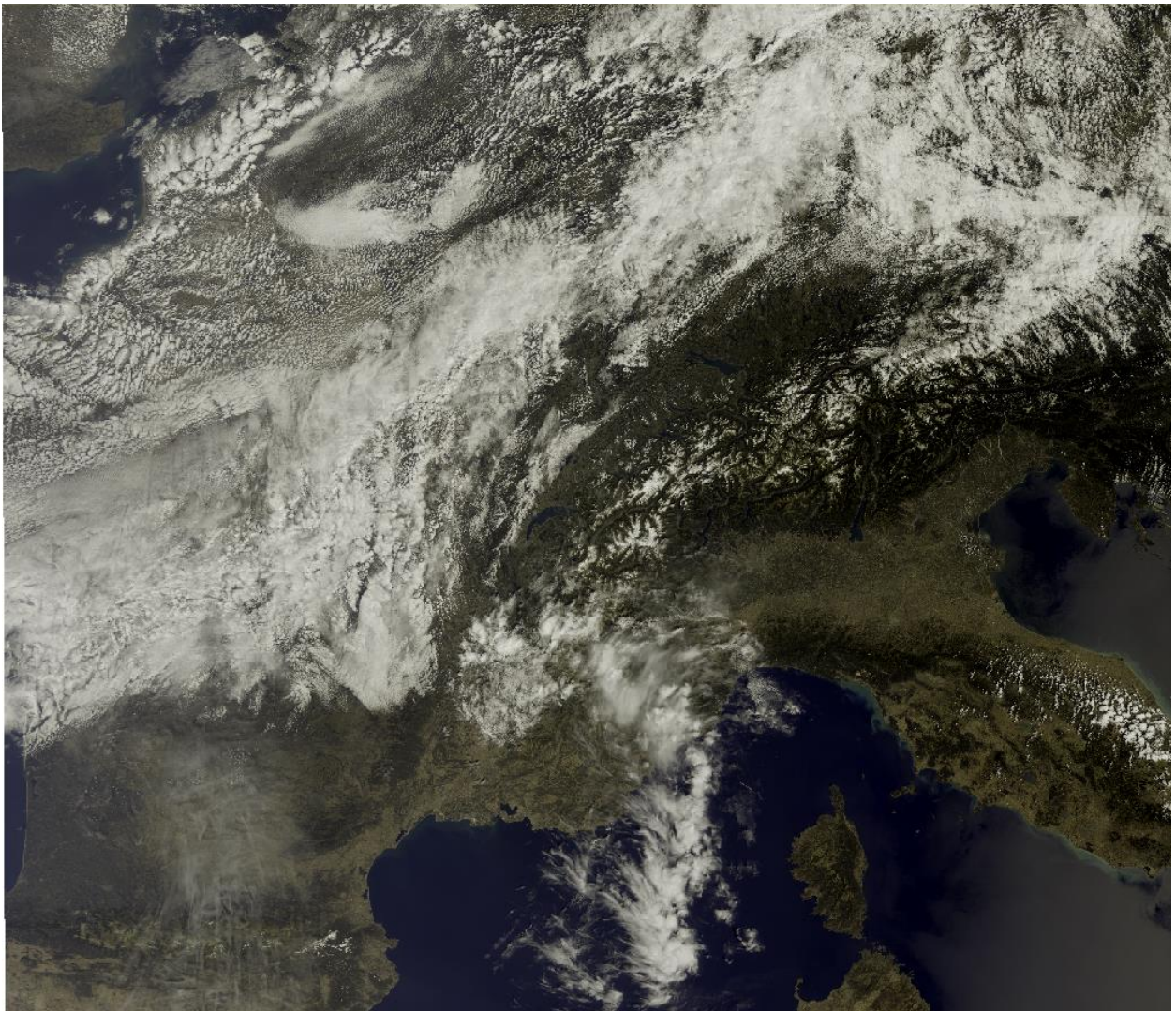


Figure 36: Level 1 FR product

(S3A_OL_1_EFR____20170813T095026_20170813T095326_20170814T132508_017.SAFE9_021_079_2160_LN1_O_NT_002.SAFE)

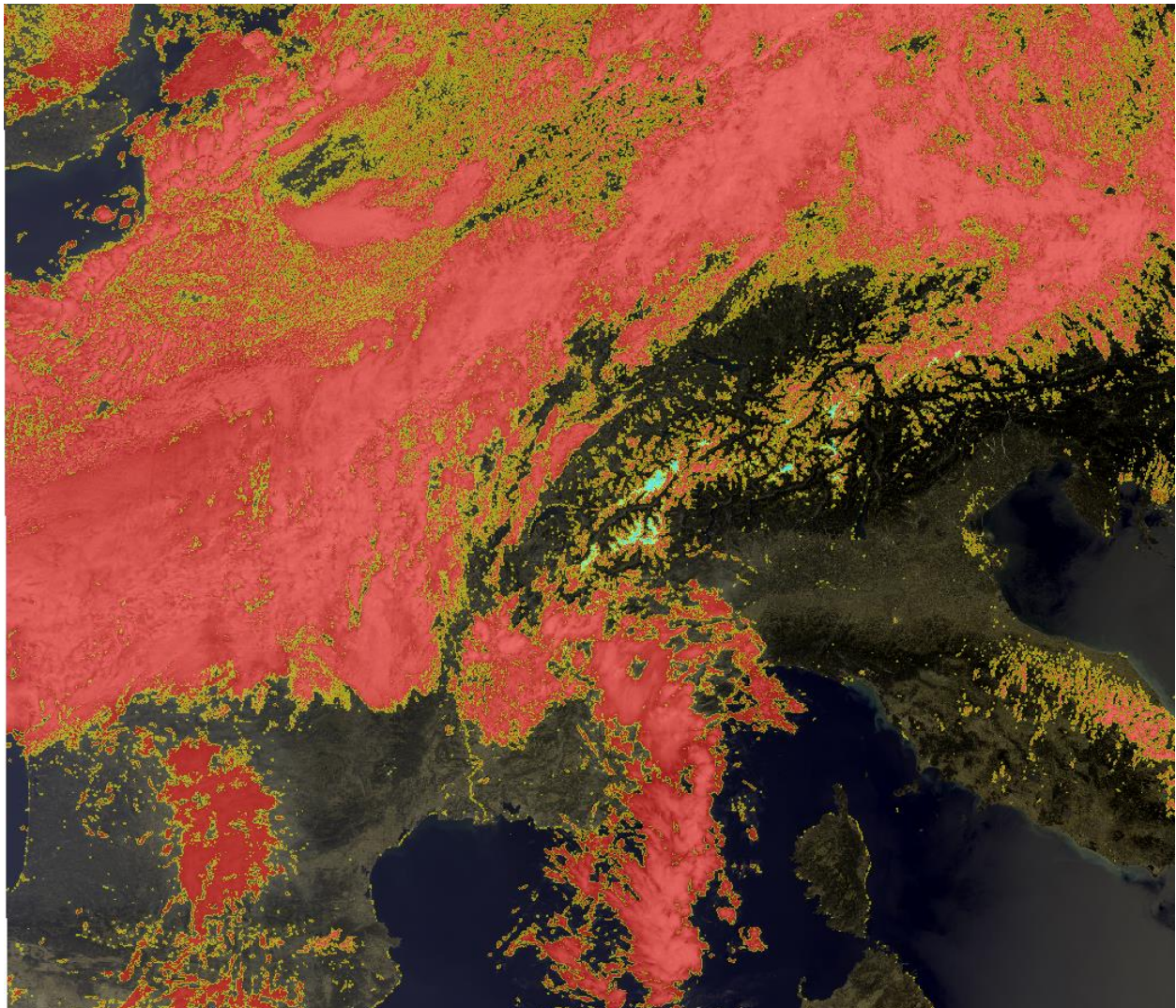


Figure 37: Level 1 FR product with corresponding Level 2 flags for cloud, cloud ambiguous, cloud margin & snow
 (S3A_OL_1_EFR____20170813T095026_20170813T095326_20170814T132508_017.SAFE9_021_079_2160_LN1_O_NT_002.SAFE)

LQSF_CLOUD	Maths		0.5	LQSF.CLOU...
LQSF_CLOUD_AMBIGUOUS	Maths		0.5	LQSF.CLOU...
LQSF_CLOUD_MARGIN	Maths		0.5	LQSF.CLOU...
LQSF_SNOW_ICE	Maths		0.5	LQSF.SNOW...

Figure 38: Level 2 flag legend

The analysis has shown that there are no anomalies or inconsistencies in the released products.

 <p>The logo for the Sentinel-3 Mission Performance Centre. It features a central blue satellite icon with the text 'SENTINEL 3' above it. To the left, there are four small square images: a sunset, a satellite view of Earth, a person in a field, and a green checkmark. To the right of the satellite icon, the text 'Mission Performance Centre' is written vertically.</p>	<p style="text-align: center;">Sentinel-3 MPC</p> <p style="text-align: center;">S3-A OLCI Cyclic Performance Report</p> <p style="text-align: center;">Cycle No. 020</p>	<p>Ref.: S3MPC.ACR.PR.01-020</p> <p>Issue: 1.0</p> <p>Date: 25/08/2017</p> <p>Page: 39</p>
---	--	--

3.3 Validation of Integrated Water Vapour over Land

There has been no update on Integrated Water Vapour over Land validation quantitative assessment during the cycle. Last figures (cycle 15) are considered valid.

Qualitative assessment by product inspection showed no detectable performance evolution.

	Sentinel-3 MPC S3-A OLCI Cyclic Performance Report Cycle No. 020	Ref.: S3MPC.ACR.PR.01-020 Issue: 1.0 Date: 25/08/2017 Page: 40
--	---	---

4 Level 2 Water products validation

4.1 [OLCI-L2-CV-210, OLCI-L2-CV-220] – Vicarious calibration of the NIR and VIS bands

There has been no update on SVC (System Vicarious Calibration) during Cycle 020.

4.2 [OLCI-L2WLR-CV-300, OLCI-L2WLR-CV-310, OLCI-L2WLR-CV-32, OLCI-L2WLR-CV-330, OLCI-L2WLR-CV-340, OLCI-L2WLR-CV-350, OLCI-L2WLR-CV-360 and OLCI-L2WLR-CV-370] – Level 2 Water-leaving Reflectance product validation.

There has been no update on Water-leaving Reflectance validation quantitative assessment during the cycle, due to issues with data availability. Last figures (cycle 19) are considered valid. Qualitative assessment by product inspection showed no detectable performance evolution.

4.3 [OLCI-L2WLR-CV530] Validation of Aerosol Product

There has been no update on Aerosol Products validation quantitative assessment during the cycle. Last figures (cycle 18) are considered valid.

Qualitative assessment by product inspection showed no detectable performance evolution.

	Sentinel-3 MPC S3-A OLCI Cyclic Performance Report Cycle No. 020	Ref.: S3MPC.ACR.PR.01-020 Issue: 1.0 Date: 25/08/2017 Page: 41
--	---	---

5 Level 2 SYN products validation

5.1 [SYN-L2-CV-100]

There has been no update on SYN products validation quantitative assessment during the cycle. Last figures (cycle 10) are considered valid.

Qualitative assessment by product inspection showed no detectable performance evolution.

	Sentinel-3 MPC S3-A OLCI Cyclic Performance Report Cycle No. 020	Ref.: S3MPC.ACR.PR.01-020 Issue: 1.0 Date: 25/08/2017 Page: 42
--	---	---

6 Events

Two OLCI Radiometric Calibration Sequences have been acquired during Cycle 020:

- ❖ S04 sequence (diffuser 1) on 22/07/2017 08:09 to 08:11 (absolute orbit 7437)
- ❖ S05 sequence (diffuser 2) on 22/07/2017 09:50 to 09:52 (absolute orbit 7438)

	Sentinel-3 MPC S3-A OLCI Cyclic Performance Report Cycle No. 020	Ref.: S3MPC.ACR.PR.01-020 Issue: 1.0 Date: 25/08/2017 Page: 43
--	---	---

7 Appendix A

Other reports related to the Optical mission are:

- ❖ S3-A SLSTR Cyclic Performance Report, Cycle No. 020 (ref. S3MPC.RAL.PR.02-020)

All Cyclic Performance Reports are available on MPC pages in Sentinel Online website, at:
<https://sentinel.esa.int>

End of document